Electronic Supplementary Material (ESI) for ChemComm.

Supporting Information for

Electrocatalytic CO_2 reduction by a cobalt bis(pyridylmonoimine) complex: effect of acid concentration on catalyst activity and stability

Weixuan Nie and Charles C. L. McCrory*

Contents:

Experimental Information

Materials

Ultrapure water (18.2 MΩ cm resistivity) was purified with a Thermo Scientific Barnstead Nanopure water purification system. Nitrogen (N_2) was boil-off gas from a liquid nitrogen source. Carbon dioxide (CO_2, medical grade, >99.0%) was purchased from Cryogenic gases. Tetrabutylammonium hexaflurophosphate ($n\text{Bu}_4\text{NPF}_6$, >98.0%) was purchased from TCI America and recrystallized from Methonal/H_2O (v/v = 8/1). 2,2,2-trifluoroethanol (TFE, ReagentPlus grade, ≥99.0%) was purchased from Sigma Aldrich. Acetonitrile (MeCN, HPLC plus, ≥99.9%) was purchased from Sigma Aldrich and used without additional purification. The typical water concentration in MeCN as received has been previously measured to be $[H_2O] \approx 0.040$ M.[S1] Nitric acid (HNO_3, 67-70% w/w, TraceMetal Grade with <1 ppb metal concentration) was purchased from Fisher Scientific. All other chemicals were purchased from commercial sources, and all chemicals were used as received unless otherwise noted.

General Methods

NMR spectra were recorded on Varian MR400 (400 MHz) spectrometers, and chemical shifts are reported in ppm relative to TMS standards. Elemental analyses were performed by Midwest Microlab, Inc. Gas chromatography measurements were conducted on a custom-designed 2-channel Thermo Scientific Trace 1310 gas chromatograph with dual TCD detectors. HPLC measurements were collected using a Thermo Scientific Dionex Ultimate 3000 series HPLC. Electrochemical experiments were conducted using a Bio-Logic/Science Instruments SP-200 potentiostat using the EC-Lab V10.44 software package. UV-Vis spectra were collected with Perkin Elmer PDA UV-Vis Lambda 265 equipment. IR spectra were collected with Thermo Scientific NICOLET iS50 FT-IR. ICP-MS data were collected using PerkinElmer NexION 2000. X-ray diffraction data was collected on a CrystalClear-SM Expert 2.0 r16 (Rigaku, 2014) with a Rigaku Saturn944+ CCD detector using Cu Kα (wavelength is 1.54 Å). The structure was solved by direct methods and refined on F2 full-matrix least-squares using SHELXL-2013 (Sheldrick, 2013).[S2]

Synthesis

Preparation of Ligand L-L. The Ligand L-L was synthesized according to literature methods.[S3] A solution of 2-acetylpyridine (1.00 g, 8.04 mmol) in 20 mL *i*-PrOH was added into a solution of ethylenediamine (0.24 g, 4.00 mmol) in 20 mL *i*-PrOH. The mixture was stirred at room temperature for 24 hours. After removing the solvent, the yellow oil residue was put into a -4 ℃ refrigerator to get a semi-solid crude product. The crude ligand was re-crystallized from 5 mL hexane to give white needles which were dried in vacuum overnight (0.70 g, 65% yield). ^{1}H NMR (CD_3Cl-d_3, 400 MHz, Fig S1): δ 8.59 (2H, d, *Ar*-H), δ 8.07 (2H, d, *Ar*-H), δ 7.69 (2H, m, *Ar*-H), δ 7.28 (2H, m, *Ar*-H), δ 3.98 (4H, s, CH_2), δ 2.44 (6H, s, CH_3).

Preparation of [Co(L-L)Br$_2$]. A 5 mL THF solution of $CoBr_2$ (87.50 mg, 0.40 mmol) was added into a 3 mL THF solution of ligand L-L (106.50 mg, 0.40 mmol) with a 1:1 metal salt : ligand molar ratio. The mixture was stirred at room temperature for 24 hours. The dark purple precipitate was collected by filtration and then washed with THF and ether three times. The product was obtained after drying in vacuum overnight (183.40 mg, 95% yield). Anal. Calcd (found) for [Co(L-L)Br$_2$], ($C_{16}H_{18}N_4CoBr_2$): %C 39.62, (38.92); %H 3.74, (3.80); %N 11.55, (11.22).

Preparation of [Co(L-L)Br$_2$]Br. Aerobic oxidation of in situ prepared [Co(L-L)Br$_2$] in the presence of 1 equiv HBr(aq) in ethanol overnight (18 hours) resulted a green solid (179.78 mg, 80% yield). Recrystallization was accomplished by diffusion of Et_2O into a MeOH solution of the green solid. Dark green crystals were obtained after a few days and kept in dark to avoid photochemical degradation. ^{1}H NMR (Trifluoroacetic acid-d_1, 400 MHz): δ 9.44 (2H, d, *Ar*-H), δ 8.28 (2H, t, *Ar*-H), δ 8.14 (2H, d, *Ar*-H), δ 7.94 (2H, t, *Ar*-H), δ 4.81 (4H, s, CH_2), δ 2.92 (6H, s, CH_3). Anal. Calcd (found) for [Co(L-L)Br$_2$]Br (C16H18N4CoBr3): %C 34.01, (34.07); %H 3.21, (3.30); %N 9.92, (9.89).

Electrochemical Methods and Product Analysis

Cyclic Voltammetry. The working electrode was a 0.071 cm^2 glassy carbon disk electrode (CH instruments), and the counter electrode was carbon rod (99.999% Strem). The reference electrode was a Ag/$AgNO_3$ (1.0 mM)/MeCN nonaqueous reference electrode (also containing 0.1 M nBu_4NPF_6), separated from the solution by a Vycor frit (Bioanalytical Systems, Inc.) and externally referenced to ferrocene. The scan rate was 50 mV/s. Prior to each set of measurements, the uncompensated solution resistance (R_u) in the cell was measured using a single-point impedance measurement at 100 kH_z with a 20 mV amplitude about the open-circuit potential. Cyclic voltammograms were automatically corrected for IR drop at 85% through positive feedback using the Bio-Logic ECLab software.

Controlled-Potential Electrolysis. The controlled-potential electrolysis experiments were conducted in a two-chamber H-cell shown in Fig S8. The left chamber held the working and reference electrodes and was filled with 20 mL of 0.3 mM catalyst solution in MeCN with 0.1 M nBu_4NPF_6. The right chamber held the counter electrode in 15 mL of a 5 mM ferrocene solution in MeCN. These two chambers were separated by a fine-porosity glass frit. The working electrode was a 3.2 cm × 1.6 cm × 0.1 cm glassy carbon plate (HTW Hochtemperatur-Werkstoff GmbH) which was half immersed in the solution. Prior to each experiment, the working electrode was first polished on 600-grit SiC polishing paper (Buehler, Ltd) and sonicated for 5 min in *i*-PrOH. The reference electrode was a Ag/$AgNO_3$ (1.0 mM)/MeCN nonaqueous reference electrode (also containing 0.1 M $n\mathrm{Bu_4NPF_6}$) separated from the solution by a Vycor frit (Bioanalytical Systems, Inc.). The counter electrode was nichrome wire (ARCOR). Prior to each electrolysis experiment, the cell was purged with CO_2 or N_2 for 30 minutes and then sealed under an atmosphere of CO or N_2. The CPE experiments were conducted with no IR compensation for solution resistance (~60 Ω), and the reported electrolysis potentials are the actual applied potentials. After each electrolysis, the headspace was sampled using a Thermo Scientific 10 mL Syringe, and the CO and H_2 concentration were measured by gas chromatography. The post-electrolysis solution was analyzed using HPLC to determine HCOOH concentration. The Faradaic efficiency of every product was calculated by dividing the measured product concentrations by the amount expected on the basis of charge passed during the CPE measurement.

Product Analysis. Gaseous products (*i.e.* CO and H_2) in the headspace were measured using a Thermo Scientific Trace 1310 with two analyzer systems. Using a valve system, column configuration, and method developed by Thermo Scientific and Custom Solutions Group LLC., gases were separated so that H_2 was detected on one channel using an Ar carrier, and all other gases were detected on a second channel using a He carrier gas. 5.0 mL aliquots of the working-electrode headspace were collected using a Thermo Scientific 10 mL Syringe. The headspace sample was injected directly into the 5 mL sample loop. Gases were detected on both channels using thermal conductivity detectors (TCDs), and chromatographs were analyzed using Thermo Scientific Dionex Chromeleon^{TM} 7.2.2.6686 Chromatography Data System software.

Liquid products (*i.e.* HCOOH) were analyzed using high-performance liquid chromatography (HPLC). HPLC measurements were collected using a Thermo Scientific Dionex Ultimate 3000 series HPLC equipped with a UV-Vis detector and refractive index detector (RID). Liquid aliquots were collected from the working-electrode chamber post-electrolysis and placed in an autosampler from which 10 μL aliquots of each liquid sample was injected into a HyperREZ XP Carbohydrate H+ column. The eluent was 0.05 M H_2SO_4 aqueous solution at a flow rate of 0.6 mL min^{-1}. The temperature of the column was maintained at 50 ℃. Products were detected using the RID detector and chromatographs were analyzed using Thermo Scientific Dionex Chromeleon^{TM} 7.2.2.6686 Chromatography Data System software.

Faradaic efficiencies were calculated by dividing the total number of moles of each product by the moles of electrons calculated from the amount of charge passed during the electrolyses normalized for the number of electrons required to produce each product.

SEM-EDS tests. All electrodes tested by SEM-EDS (JEOL-7800FLV FE) were not rinsed post electrolysis. The SEM images showing the morphology of the electrode surface were recorded with a field emission gun scanning electron microscope at 18 kV, equipped with an energy dispersive X-ray (EDS) detector. The EDS analyses were conducted using an SEM acceleration voltage of 18 kV.

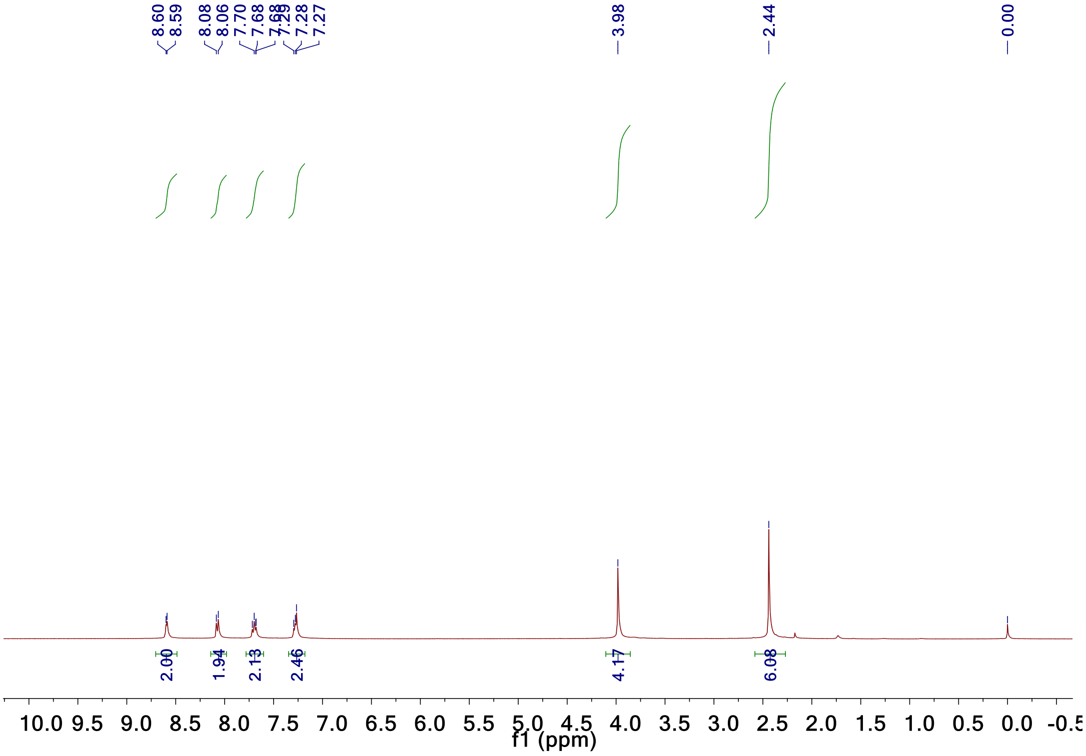

Figure S1. ^{1}H-NMR Spectrum of Ligand **L-L** in CD_3Cl-d_3 (δ 7.69 solvent residual peak)

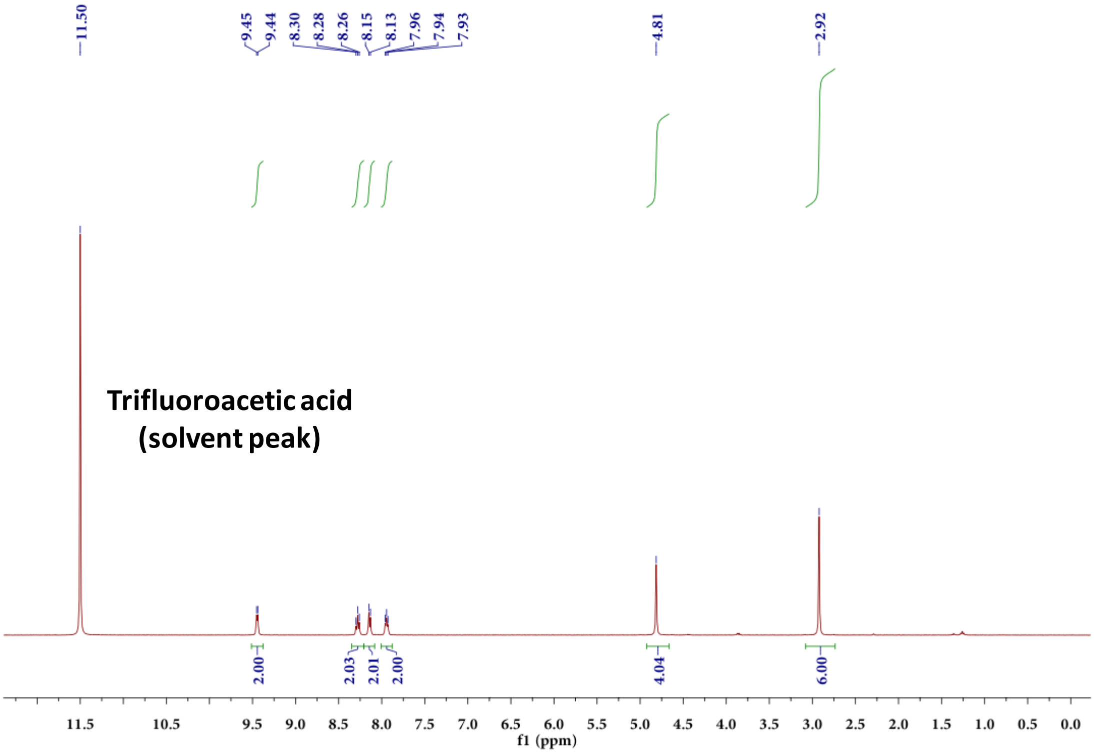

Figure S2. ^{1}H-NMR Spectrum of **[Co(L-L)Br$_2$]Br** in Trifluoroacetic acid-d_1 (δ=11.5 solvent residual peak)

Table S1. Crystal data and structure refinement for the cobalt complex catalyst

Formula	**[Co(L-L]Br$_2$]Br** ($C_{16}H_{18}Br_3CoN_4$)
FW	565.00
Crystal system	triclinic
Space group	P *-1*
a (Å)	8.2736(4)
b (Å)	10.7007(5)
c (Å)	11.1674(4)
α (deg)	85.313(4)
β (deg)	71.078(4)
γ (deg)	86.856(4)
Z	2
Volume (Å^3)	931.71(7)
Temperature (K)	293(2)
Density (g/mL)	2.014
Reflections collected / unique	13611 / 3345 [R(int) = 0.0293]
Final R indices [I>2sigma(I)]	R1 = 0.0252, wR2 = 0.0637
R indices (all data)	R1 = 0.0254, wR2 = 0.0638
Goodness-of-fit on F^2	1.005

Table S2. Related bond lengths and bond angles of the cobalt complex catalyst

Bonds	**/ Å**
Co(1)-N(3)	1.865(2)
Co(1)-N(2)	1.868(2)
Co(1)-N(4)	1.961(2)
Co(1)-N(1)	1.971(2)
Co(1)-Br(2)	2.3906(4)
Co(1)-Br(1)	2.4047(4)

Bond angles	**/ deg**
N(3)-Co(1)-N(2)	85.81(9)
N(3)-Co(1)-N(4)	82.78(9)
N(2)-Co(1)-N(4)	167.50(9)
N(3)-Co(1)-N(1)	167.50(9)
N(2)-Co(1)-N(1)	82.52(9)
N(4)-Co(1)-N(1)	109.22(9)
N(3)-Co(1)-Br(2)	91.40(6)
N(2)-Co(1)-Br(2)	88.44(6)
N(4)-Co(1)-Br(2)	86.76(6)
N(1)-Co(1)-Br(2)	92.75(6)
N(3)-Co(1)-Br(1)	87.00(6)
N(2)-Co(1)-Br(1)	92.69(6)
N(4)-Co(1)-Br(1)	91.79(6)
N(1)-Co(1)-Br(1)	89.08(6)
Br(2)-Co(1)-Br(1)	177.965(19)

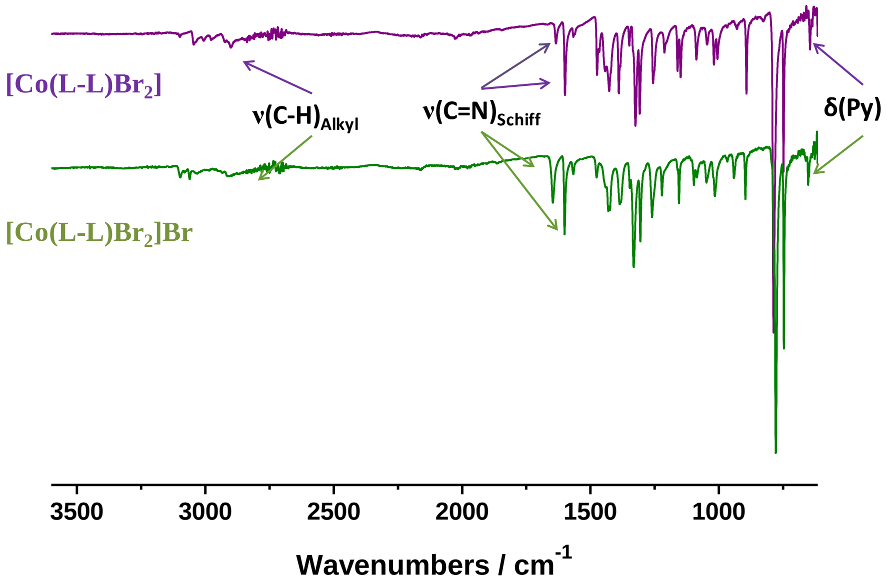

Figure S3. IR Spectrum of **[Co(L-L)Br$_2$]** and **[Co(L-L)Br$_2$]Br**

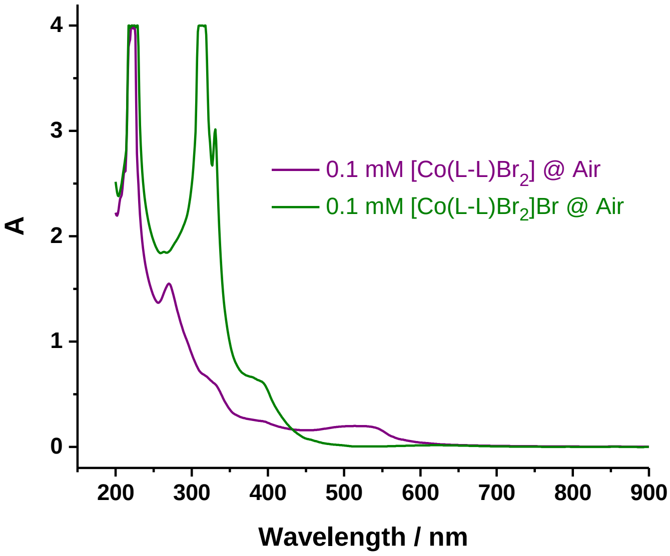

Figure S4. UV-vis spectrum of 0.1 mM **[Co(L-L)Br$_2$]** and **[Co(L-L)Br$_2$]Br** in MeCN in air. Based on UV-vis spectra of Co complexes adopting similar structures reported in literatures[S3, S18, S19], the intense peaks at 221 nm and 270 nm (for **[Co(L-L)Br$_2$]**), 221 nm and 313 nm (for **[Co(L-L)Br$_2$]Br**) were assigned to ligand π→π* transition. The peak at 528 nm in **[Co(L-L)Br$_2$]** spectrum was assigned to Co^{2+} *d-d* transition ($^4T_{1g}(F) \rightarrow {}^4T_{1g}(P)$), which is not observed in **[Co(L-L)Br$_2$]Br** spectrum.

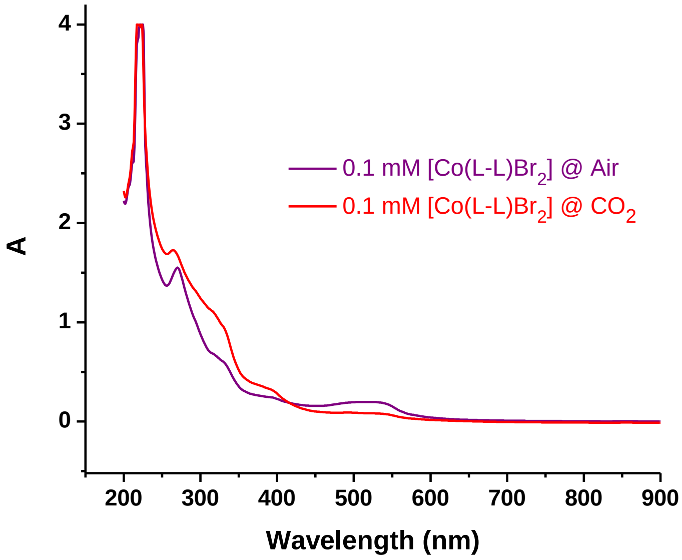

Figure S5. UV-vis spectrum of 0.1 mM **[Co(L-L)Br$_2$]** in MeCN in air and under CO_2. CO_2 has little influence on UV-vis spectrum of 0.1mM **[Co(L-L)Br$_2$]** in MeCN.

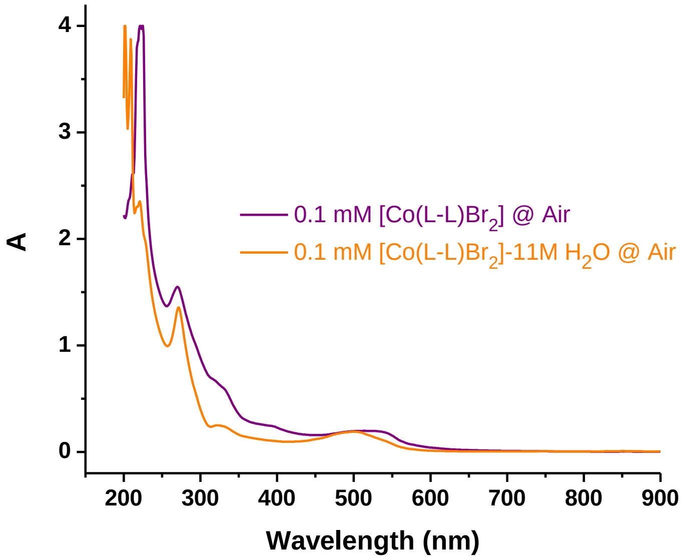

Figure S6. UV-vis spectrum of 0.1 mM **[Co(L-L)Br$_2$]** in MeCN in air and with 11 M H_2O in air. Proton source H_2O has little influence on UV-vis spectrum of 0.1 mM **[Co(L-L)Br$_2$]** in MeCN.

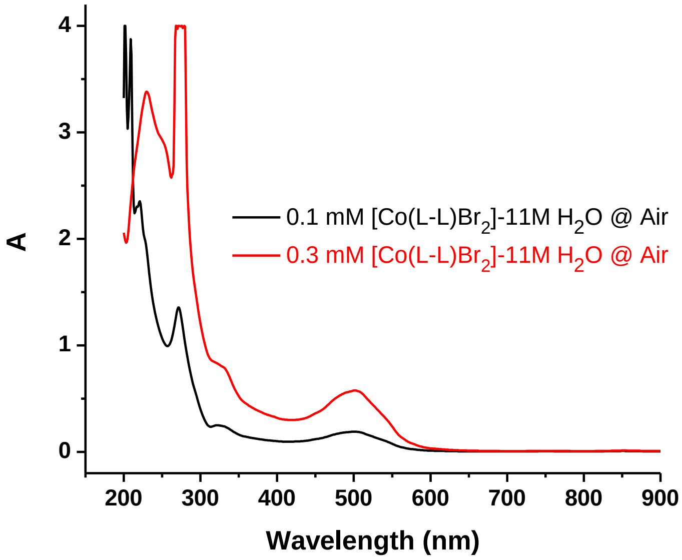

Figure S7. UV-vis spectrum of 0.1 mM (black curve) and 0.3 mM (red curve) **[Co(L-L)Br$_2$]** in MeCN in air. The concentration of **[Co(L-L)Br$_2$]** affects absorption features of ligand π→π* transition but has little influence on Co^{2+} *d-d* transition. The concentration 0.3 mM was used consistently in the following electrolysis experiments.

Paramagnetic Susceptibility Measurements (Evans Method)

The measurement of paramagnetic susceptibility

The paramagnetic susceptibility of [Co(L-L)]Br$_2$ was studied by Evans method which was established in 1959 for paramagnetic susceptibility measurement by using NMR[S20]. The most commonly used equation is

$$\chi_{mass} = \frac{3\Delta f}{4\pi f c} + \chi_0 + \frac{\chi_0(d_0 - d_s)}{c}$$

$$\chi_{mol} = M\chi_{mass}$$

Where χ_{mass} is mass susceptibility $(cm^3 \cdot g^{-1})$, χ_{mol} is molar susceptibility $(cm^3 \cdot mol^{-1})$, Δf is observed frequency difference (Hz), f is spectrometer frequency $(400 \times 10^6 Hz)$, c is concentration of the sample solution $(g \cdot cm^{-3})$, χ_0 is mass susceptibility of solvent DMSO $(-0.68 \times 10^{-6} cm^3 \cdot g^{-1})$, d_0 is density of solvent $(g \cdot cm^{-3})$, d_s is density of solution $(g \cdot cm^{-3})$, M is molecular weight of [Co(L-L)]Br$_2$ (485.08 $g \cdot mol^{-1}$). In the most cases, the density of the solution is almost the same as the density of the solvent. So the equation is usually

$$\chi_{mass} = \frac{3\Delta f}{4\pi f c} + \chi_0$$

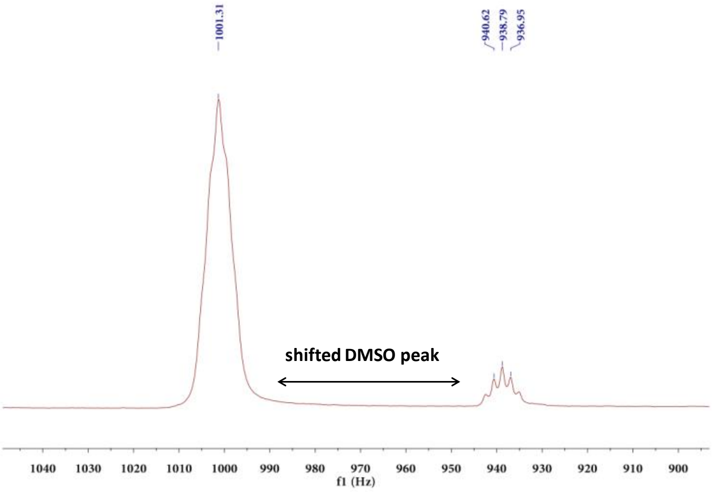

Figure S8. The shifted DMSO peaks in ^{1}H-NMR Spectrum of 2.0 mg **[Co(L-L)Br$_2$]** in 0.55 mL d_6-DMSO

Table S3. The paramagnetic susceptibility of [Co(L-L)]Br$_2$ calculated based on Evans Method

$m(sample)/g$	$V(d_6DMSO)/cm^3$	$[sample]/g \cdot ml^{-1}$	$\chi_{mass}/cm^3 \cdot g$	$\chi_{mol}/cm^3 \cdot mol$
0.0028	0.55	0.0051	8.7×10^{-6}	4.2×10^{-3}
0.0022	0.55	0.0040	7.5×10^{-6}	3.6×10^{-3}
0.0020	0.55	0.0036	9.6×10^{-6}	4.7×10^{-3}
		Average		4.2×10^{-3}

The number of unpaired electrons

Based on Curie's Law,

$$\chi_{mol}T = constant\ for\ a\ simple\ paramagnet$$

$$\chi_{mol}T = \frac{1}{2}[S(S+1)] = 8n(n+2)$$

$$\mu_{eff} = \sqrt{8(\chi_{mol}T)} = 2\sqrt{S(S+1)} = \sqrt{n(n+2)}$$

Where T is temperature (K), S is total spin quantum number, n is the number of unpaired electrons, μ_{eff} is effective magnetic moment ($Bohr\ magneton, \mu_B$), which is independent of temperature.

Table S4. the calculated μ_{eff} and n in [Co(L-L)]Br$_2$ at 293K based on χ_{mol}

$\chi_{mol}/cm^3 \cdot mol$	$\chi_{mol}T$	μ_{eff}	n	μ_{eff} *in literature*[S3]	n *in literature*[S3]
4.2×10^{-3}	1.22	3.12	2.28	2.85	2.02

The effective magnetic moment μ_{eff} 3.12 matches the value 2.85 reported in the literature.[S3] Based on the calculation [Co(L-L)]Br$_2$ shows μ_{eff} between the value ca. 1.73 for a pure octahedral low spin state and 3.87 for a pure octahedral high spin state. This could be explained by the occurrence of a thermal equilibrium between these two spin states at the room temperature.[S3]

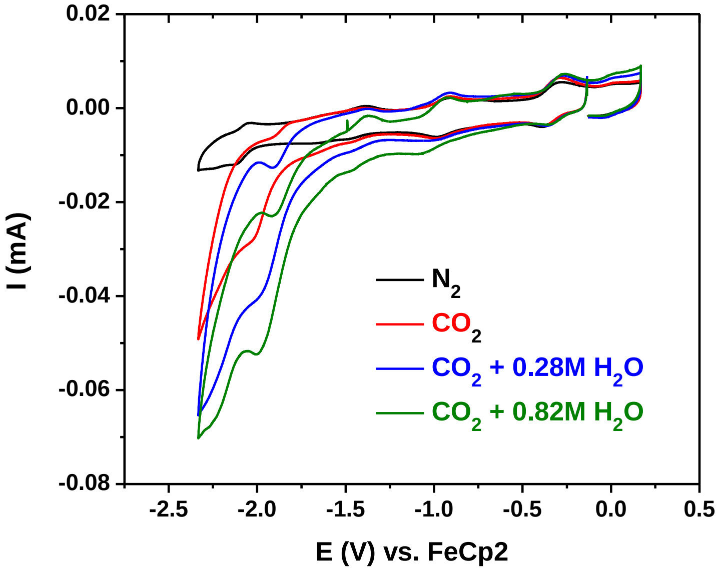

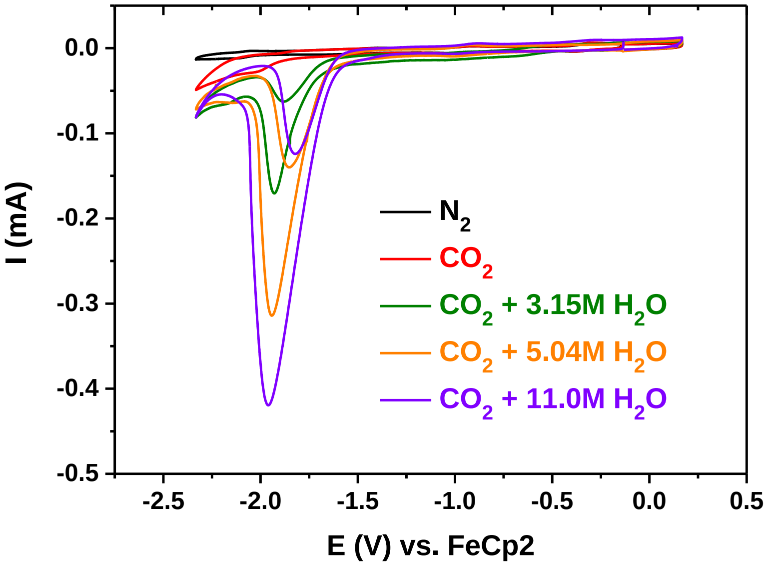

Figure S9. CVs of 0.3 mM **[Co(L-L)Br$_2$]** in acetonitrile with 0.1 M *n*Bu$_4$NPF$_6$ with increasing H_2O concentration

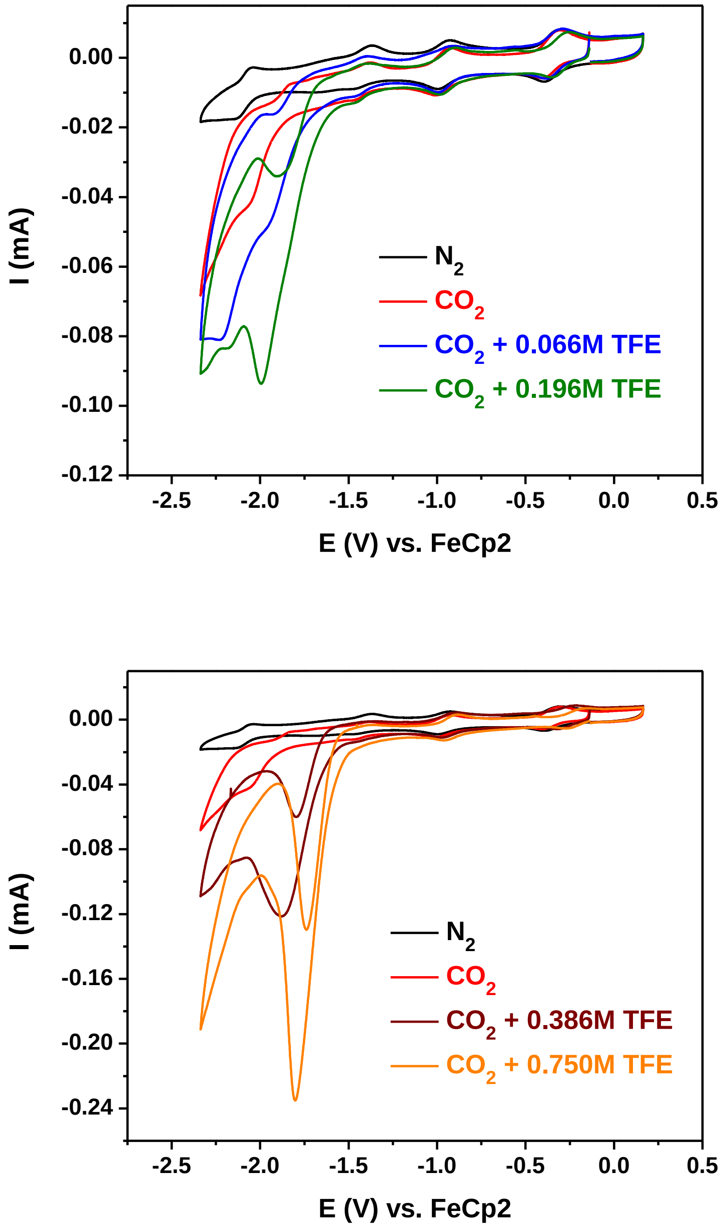

Figure S10. CVs of 0.3 mM **[Co(L-L)Br$_2$]** in acetonitrile with 0.1 M *n*Bu$_4$NPF$_6$ with increasing TFE concentration

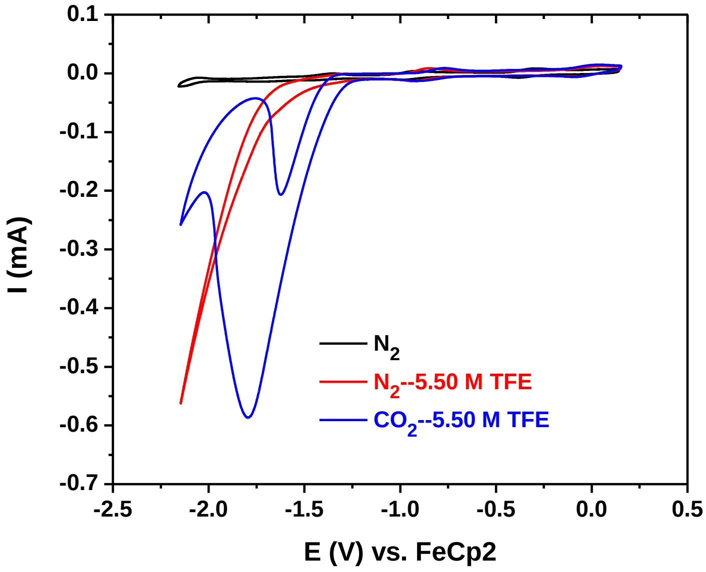

Figure S11. CVs of 0.3 mM **[Co(L)Br$_2$]** in acetonitrile with 0.1 M *n*Bu$_4$NPF$_6$ under N$_2$ and CO$_2$ with TFE.

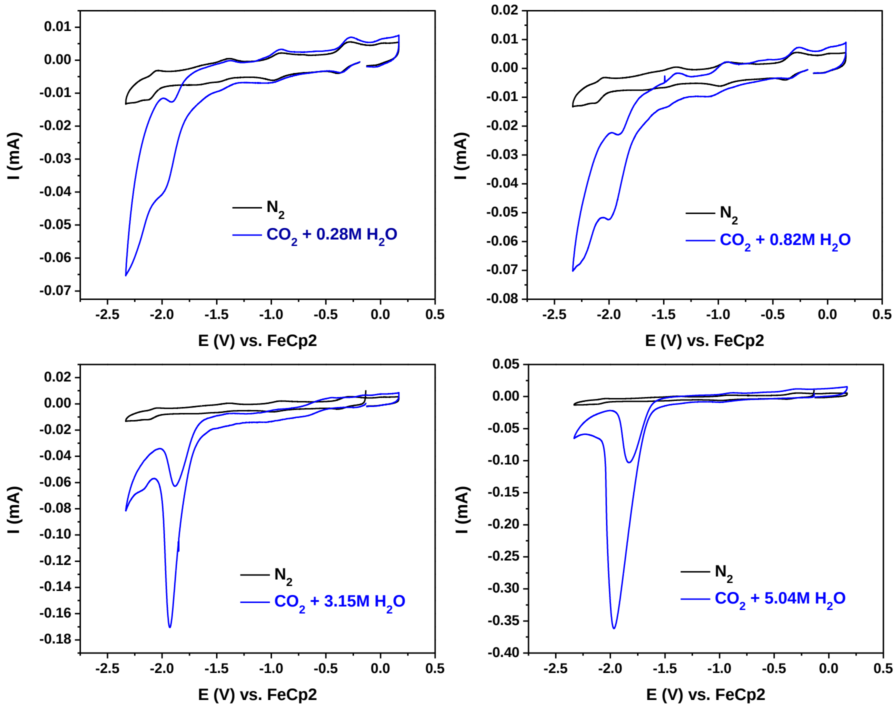

Figure S12. CVs of 0.3 mM **[Co(L-L)Br$_2$]** in acetonitrile with 0.1 M *n*Bu$_4$NPF$_6$ under N$_2$ and CO$_2$ with different H$_2$O concentrations to show that the inverted peak shape is attributed to the overlap of the catalytic current response for CO$_2$ reduction with the more negative, reversible Co$^{1+/0}$ redox feature.

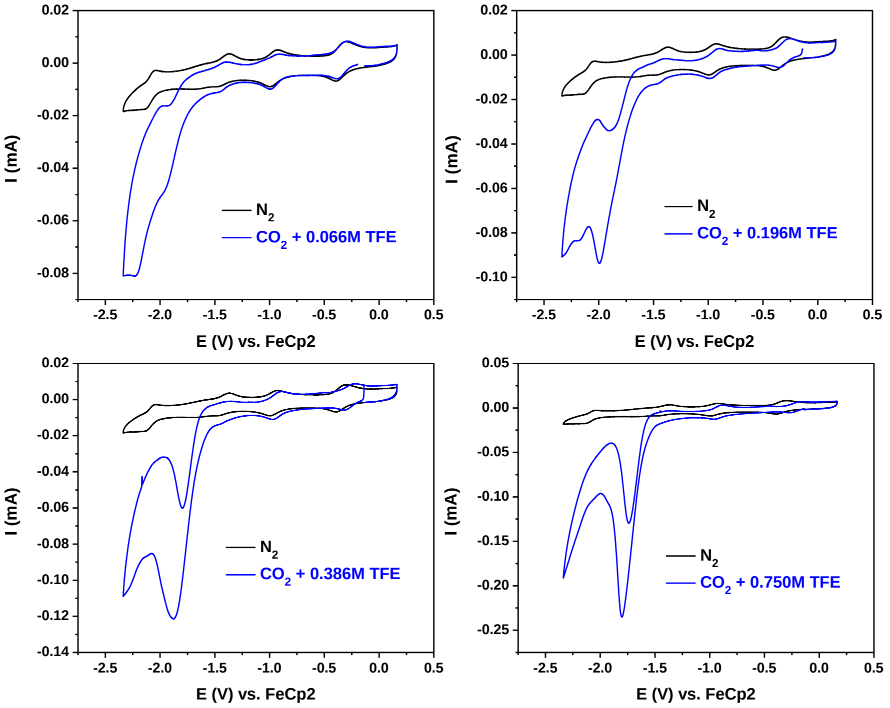

Figure S13. CVs of 0.3 mM **[Co(L-L)Br$_2$]** in acetonitrile with 0.1 M *n*Bu$_4$NPF$_6$ under N$_2$ and CO$_2$ with different TFE concentrations to show that the inverted peak shape is attributed to the overlap of the catalytic current response for CO$_2$ reduction with the more negative, reversible Co$^{1+/0}$ redox feature.

Figure S14. The Controlled-Potential Electrolysis cell setup

Table S5. Conditions and Product Analysis of the Controlled Potential Electrolysis for CO_2 reduction with 0.3 mM Co(L-L)Br_2

Entry	E / V vs. $FeCp_2$	[Proton source] / M	Charge / C	Faradaic Efficiency / %			Co / wt%[a]
				CO	H_2	HCOOH	
0	-1.95	-	2.2 ± 0.3	2.8 ± 2.7	0	6.3 ± 2.6	0.52
1-a	-1.95	[H_2O] 0.55 M	2.2 ± 0.5	7.0 ± 2.9	0	7.5 ± 3.8	-[b]
1-b	-1.95	[H_2O] 1.10 M	3.4 ± 0.4	16.3 ± 5.1	0	4.5 ± 1.1	-[b]
1-c	-1.95	[H_2O] 2.75 M	5.2 ± 0.3	56.5 ± 11.5	0	3.4 ± 0.8	-[b]
1-d	-1.95	[H_2O] 5.50 M	7.1 ± 0.7	67.4 ± 11.0	0.3 ± 0.1	1.9 ± 0.5	-[b]
1	-1.95	[H_2O] 11.00 M	8.3 ± 0.9	80.5 ± 4.7	1.1 ± 0.5	0.7 ± 0.3	0.3
2-a	-1.85	[TFE] 0.275 M	3.4 ± 0.6	13.6 ± 1.7	0	5.6 ± 2.4	-[b]
2-b	-1.85	[TFE] 0.55 M	4.0 ± 0.4	34.7 ± 1.4	0	4.0 ± 0.3	-[b]
2-c	-1.85	[TFE] 1.10 M	6.2 ± 1.1	65.8 ± 5.2	0	2.2 ± 1.1	0.13
2-d	-1.85	[TFE] 2.75 M	11.2 ± 3.0	75.4 ± 1.0	1.3 ± 1.2	0.7 ± 0.6	0.01
2	-1.85	[TFE] 5.50 M	10.1 ± 2.3	87.7 ± 8.2	1.7 ± 0.7	0	0.01

[a] Weight percent of Co deposited onto the electrode post-electrolysis as measured by SEM-EDS. [b] Not measured.

Table S6. Conditions and Product Analysis of the CPE control groups for CO_2 reduction

Entry	Catalyst / 0.3 mM	E/V vs. $FeCp_2$	[Proton source] / M	Charge / C	Faradaic Efficiency / %[a]		Co / wt%[b]
					CO	H_2	
1-A	$CoBr_2$	-1.95	[H_2O] 11.00 M	2.0 ± 0.1	0	24.5 ± 13.6	7.2
2-A	$CoBr_2$	-1.85	[TFE] 5.5 M	6.2 ± 1.3	0	21.5 ± 13.0	0.45
1-B	Glassy Carbon	-1.95	[H_2O] 11.00 M	2.0 ± 0.1	0	20.2 ± 4.1	-[c]
2-B	Glassy Carbon	-1.85	[TFE] 5.5 M	3.8 ± 1.2	0	20.1 ± 12.0	-[c]
1-C	Ligand	-1.95	[H_2O] 11.00 M	2.9 ± 0.3	3.5 ± 3.2	6.6 ± 3.4	-[c]

[a] No HCOOH was detected after electrolysis with control groups. [b] Weight percent of Co deposited onto the electrode post-electrolysis as measured by SEM-EDS. [c] Not measured.

Table S7. Conditions and Product Analysis of the CPE control groups for CO_2 reduction at different potentials.

E / V vs. $FeCp_2$	**[Proton source] / M**	**Charge / C**	**Faradaic Efficiency / %**			**Co / wt%[a]**
			CO	**H_2**	**HCOOH**	
No proton source						
-1.95	0	2.2 ± 0.3	2.8 ± 2.7	0	6.3 ± 2.6	0.52%
-2.15	0	4.3 ± 1.4	4.2 ± 1.7	0	2.7 ± 0.9	0.52%
Water						
-1.75	11.00 M	3.1 ± 0.3	30.3 ± 10.8	6.4 ± 1.8	0	0.97%
-1.95	11.00 M	8.3 ± 0.9	80.5 ± 4.7	1.1 ± 0.5	0.7 ± 0.3	0.35%
-2.15	11.00 M	16.2 ± 2.5	104.3 ± 5.5	0.7 ± 0.4	0	0.18%
-2.35	11.00 M	17.0 ± 0.6	44.3 ± 12.2	45.5 ± 2.5	0	0.54%
TFE						
-1.85	5.5 M	10.1 ± 2.3	87.7 ± 8.2	1.7 ± 0.7	0	0.01%
-2.05	5.5 M	16.8 ± 2.5	102.7 ± 3.1	1.0 ± 0.4	0	0.007%

[a] Weight percent of Co deposited onto the electrode post-electrolysis as measured by SEM-EDS.

ICP-MS tests

Deposits on the surface of unrinsed glassy carbon (GC) electrode after electrolysis were digested in 3.0 mL TraceMetal Grade HNO_3. The resulting acidic solution was first diluted to a 10.0 mL stock solution with 18 MΩ water, and then a final test solution for ICP-MS measurements was made by diluting 10 uL stock solution into 10.0 mL with 18 MΩ water. All ICP-MS measurements were corrected for an HNO_3 background at the same concentration as the test solutions.

The fraction of the catalyst [Co(L-L)]Br_2 decomposed on the electrode surface could be calculated based on the following equations:

$$n(Co)_{on\ electrode\ surface} = \frac{[Co]_{ICP-MS}\ \times 10^{-6}\ \left(\frac{g}{L}\right) \times 1000 \times 0.01(L)}{58.93\ \left(\frac{g}{mol}\right)}$$

$$Fraction = \frac{n(Co)_{on\ electrode\ surface}}{([Cat] \times V_{solution})}$$

Where $[Co]_{ICP-MS}$ is Co concentration in ICP-MS test solution after correction, $[Cat]$ is [Co(L-L)]Br_2 concentration in the electrolysis solution, $V_{solution}$ is the volume of the electrolysis solution.

Table.S8. ICP-MS results of Co content on the surface of GC electrode after electrolysis

Electrode, [proton source], potential vs. Fc$^{+/0}$	[Co] in ICP-MS test solution / ppb (as measured)	n(Co) on electrode surface / mol	Calculated fraction of [Co(L-L)Br2] decomposed on the electrode surface
GC1, no H2O, -1.95 V	2.98	5.06×10^{-7}	8.43 %
GC2, no H2O, -1.95 V	2.95	5.01×10^{-7}	8.34 %
GC3, no H2O, -1.95 V	3.14	5.31×10^{-7}	8.86 %
Average		**$5.13 \pm 0.17 \times 10^{-7}$**	**8.54 ± 0.28 %**
GC4, 11 M H_2O, -1.95 V	2.801	4.75×10^{-7}	7.91 %
GC5, 11 M H_2O, -1.95 V	2.424	4.11×10^{-7}	6.85 %
GC6, 11 M H_2O, -1.95 V	1.933	3.28×10^{-7}	5.46 %
GC7, 11 M H_2O, -1.95 V	2.46	4.16×10^{-7}	6.94 %
GC8, 11 M H_2O, -1.95 V	2.67	4.54×10^{-7}	7.56 %
Average		**$4.17 \pm 0.56 \times 10^{-7}$**	**6.94 ± 0.94 %**
GC9 (5.5M TFE, -1.85V)	1.034	1.75×10^{-7}	2.92 %
GC10 (5.5M TFE, -1.85V)	1.750	2.97×10^{-7}	4.94 %
GC11 (5.5M TFE, -1.85V)	1.069	1.81×10^{-7}	3.02 %
GC12 (5.5M TFE, -1.85V)	1.491	2.53×10^{-7}	4.21 %
GC13 (5.5M TFE, -1.85V)	1.405	2.38×10^{-7}	3.97 %
Average		**$2.29 \pm 0.51 \times 10^{-7}$**	**3.81 ± 1.14 %**

[a] [Co] in ICP-MS test solution (after correction) = [Co] in ICP-MS test solution - [Co] background

Note that a [Co] concentration of 0.927 ppb, n(Co) = 1.57×10^{-7} mol, was measured from the ICP-MS test solution of a bare GC electrode without electrolysis, suggesting some residual Co exists on the electrodes after polishing and before electrolysis.

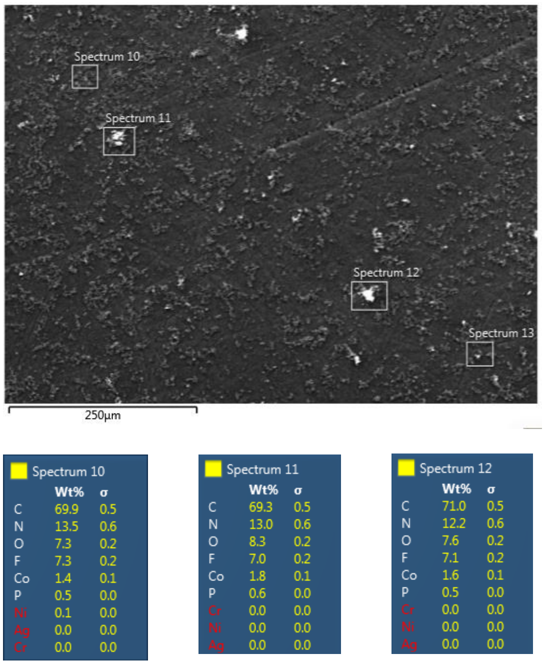

Spectrum 10

	Wt%	σ
C	69.9	0.5
N	13.5	0.6
O	7.3	0.2
F	7.3	0.2
Co	1.4	0.1
P	0.5	0.0
Ni	0.1	0.0
Ag	0.0	0.0
Cr	0.0	0.0

Spectrum 11

	Wt%	σ
C	69.3	0.5
N	13.0	0.6
O	8.3	0.2
F	7.0	0.2
Co	1.8	0.1
P	0.6	0.0
Cr	0.0	0.0
Ni	0.0	0.0
Ag	0.0	0.0

Spectrum 12

	Wt%	σ
C	71.0	0.5
N	12.2	0.6
O	7.6	0.2
F	7.1	0.2
Co	1.6	0.1
P	0.5	0.0
Cr	0.0	0.0
Ni	0.0	0.0
Ag	0.0	0.0

Figure S15. SEM-EDS analysis of a representative working electrode surface after a 30-minute CO_2RR electrolysis using 0.3 mM [Co(L-L)Br_2] with 0.1 M *n*Bu_4PF_6 in acetonitrile at -1.95 V vs. Fc/Fc^+

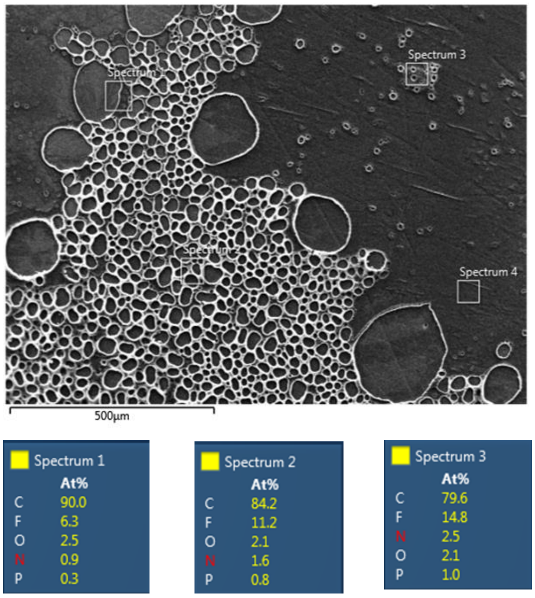

Spectrum 1

	At%
C	90.0
F	6.3
O	2.5
N	0.9
P	0.3

Spectrum 2

	At%
C	84.2
F	11.2
O	2.1
N	1.6
P	0.8

Spectrum 3

	At%
C	79.6
F	14.8
N	2.5
O	2.1
P	1.0

Figure S16. SEM-EDS analysis of a representative working electrode surface after a 30-minute CO_2RR electrolysis using 0.3 mM Ligand L-L in acetonitrile with 11.00 M H_2O and 0.1 M *n*Bu_4PF_6 in acetonitrile at -1.95 V vs. Fc/Fc^+

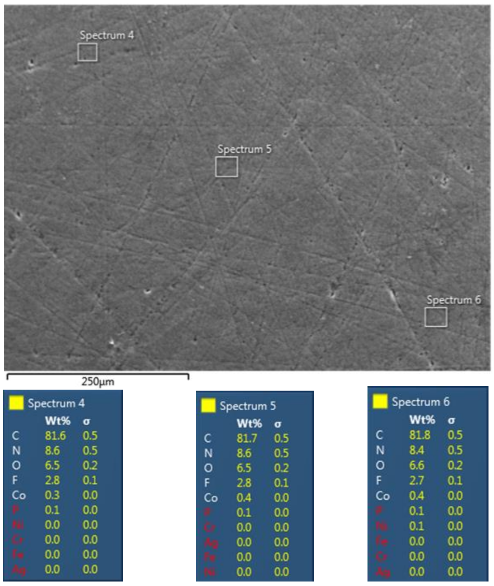

Spectrum 4	Wt%	σ
C	81.6	0.5
N	8.6	0.5
O	6.5	0.2
F	2.8	0.1
Co	0.3	0.0
P	0.1	0.0
Ni	0.0	0.0
Cr	0.0	0.0
Fe	0.0	0.0
Ag	0.0	0.0

Spectrum 5	Wt%	σ
C	81.7	0.5
N	8.6	0.5
O	6.5	0.2
F	2.8	0.1
Co	0.4	0.0
P	0.1	0.0
Cr	0.0	0.0
Ag	0.0	0.0
Fe	0.0	0.0
Ni	0.0	0.0

Spectrum 6	Wt%	σ
C	81.8	0.5
N	8.4	0.5
O	6.6	0.2
F	2.7	0.1
Co	0.4	0.0
P	0.1	0.0
Ni	0.1	0.0
Fe	0.0	0.0
Cr	0.0	0.0
Ag	0.0	0.0

Figure S17. SEM-EDS analysis of a representative working electrode surface after a 30-minute CO_2RR electrolysis using 0.3 mM [Co(L-L)Br_2] with 11.00 M H_2O and 0.1 M *n*Bu_4PF_6 in acetonitrile at -1.95 V vs. Fc/Fc$^+$

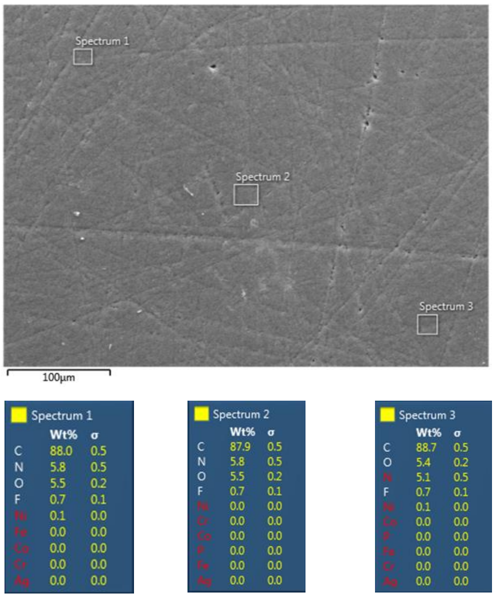

Spectrum 1	Wt%	σ
C	88.0	0.5
N	5.8	0.5
O	5.5	0.2
F	0.7	0.1
Ni	0.1	0.0
Fe	0.0	0.0
Co	0.0	0.0
Cr	0.0	0.0
Ag	0.0	0.0

Spectrum 2	Wt%	σ
C	87.9	0.5
N	5.8	0.5
O	5.5	0.2
F	0.7	0.1
Ni	0.0	0.0
Cr	0.0	0.0
Co	0.0	0.0
P	0.0	0.0
Fe	0.0	0.0
Ag	0.0	0.0

Spectrum 3	Wt%	σ
C	88.7	0.5
O	5.4	0.2
N	5.1	0.5
F	0.7	0.1
Ni	0.1	0.0
Co	0.0	0.0
P	0.0	0.0
Fe	0.0	0.0
Cr	0.0	0.0
Ag	0.0	0.0

Figure S18. SEM-EDS analysis of a representative working electrode surface after a 30-minute CO_2RR electrolysis using 0.3 mM [Co(L-L)Br_2] with 5.50 M TFE and 0.1 M *n*Bu_4PF_6 in acetonitrile at -1.85 V vs. Fc/Fc$^+$

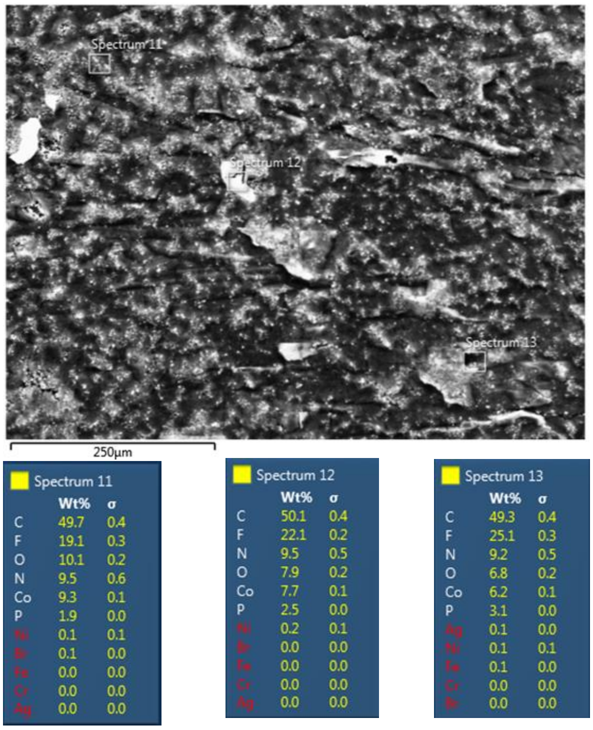

Spectrum 11	Wt%	σ
C	49.7	0.4
F	19.1	0.3
O	10.1	0.2
N	9.5	0.6
Co	9.3	0.1
P	1.9	0.0
Ni	0.1	0.1
Br	0.1	0.0
Fe	0.0	0.0
Cr	0.0	0.0
Ag	0.0	0.0

Spectrum 12	Wt%	σ
C	50.1	0.4
F	22.1	0.2
N	9.5	0.5
O	7.9	0.2
Co	7.7	0.1
P	2.5	0.0
Ni	0.2	0.1
Br	0.0	0.0
Fe	0.0	0.0
Cr	0.0	0.0
Ag	0.0	0.0

Spectrum 13	Wt%	σ
C	49.3	0.4
F	25.1	0.3
N	9.2	0.5
O	6.8	0.2
Co	6.2	0.1
P	3.1	0.0
Ag	0.1	0.0
Ni	0.1	0.1
Fe	0.1	0.0
Cr	0.0	0.0
Br	0.0	0.0

Figure S19. SEM-EDS analysis of a representative working electrode surface after a 30-minute CO_2RR electrolysis using 0.3 mM $CoBr_2$ with 11.00 M H_2O and 0.1 M $n$$Bu_4PF_6$ in acetonitrile at -1.95 V vs. Fc/Fc^+

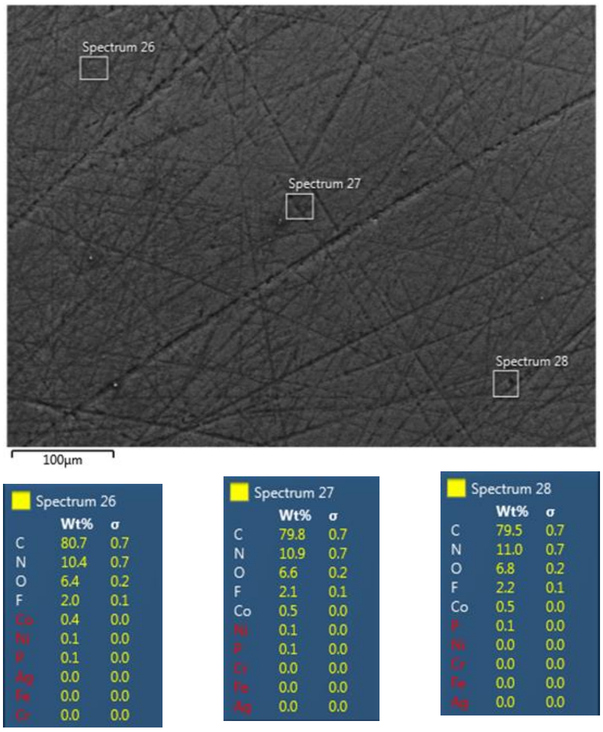

Spectrum 26	Wt%	σ
C	80.7	0.7
N	10.4	0.7
O	6.4	0.2
F	2.0	0.1
Co	0.4	0.0
Ni	0.1	0.0
P	0.1	0.0
Ag	0.0	0.0
Fe	0.0	0.0
Cr	0.0	0.0

Spectrum 27	Wt%	σ
C	79.8	0.7
N	10.9	0.7
O	6.6	0.2
F	2.1	0.1
Co	0.5	0.0
Ni	0.1	0.0
P	0.1	0.0
Cr	0.0	0.0
Fe	0.0	0.0
Ag	0.0	0.0

Spectrum 28	Wt%	σ
C	79.5	0.7
N	11.0	0.7
O	6.8	0.2
F	2.2	0.1
Co	0.5	0.0
P	0.1	0.0
Ni	0.0	0.0
Cr	0.0	0.0
Fe	0.0	0.0
Ag	0.0	0.0

Figure S20. SEM-EDS analysis of a representative working electrode surface after a 30-minute CO_2RR electrolysis using 0.3 mM $CoBr_2$ with 5.50 M TFE and 0.1 M $n$$Bu_4PF_6$ in acetonitrile at -1.85 V vs. Fc/Fc^+

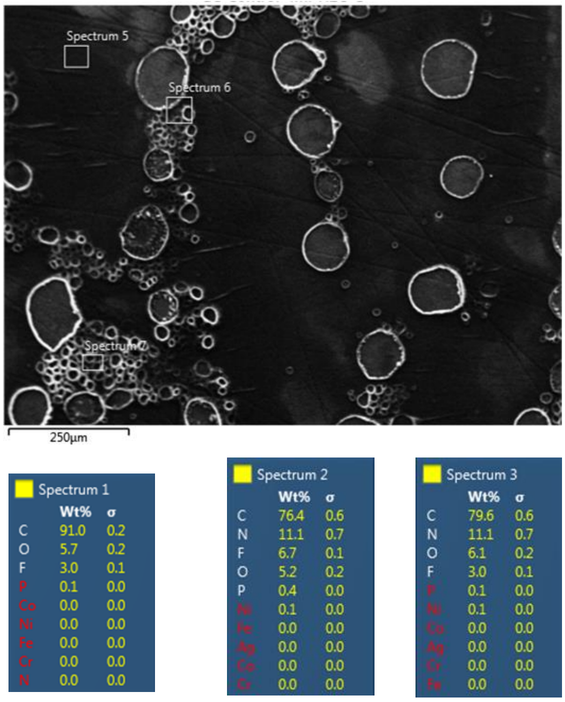

Spectrum 1

	Wt%	σ
C	91.0	0.2
O	5.7	0.2
F	3.0	0.1
P	0.1	0.0
Co	0.0	0.0
Ni	0.0	0.0
Fe	0.0	0.0
Cr	0.0	0.0
N	0.0	0.0

Spectrum 2

	Wt%	σ
C	76.4	0.6
N	11.1	0.7
F	6.7	0.1
O	5.2	0.2
P	0.4	0.0
Ni	0.1	0.0
Fe	0.0	0.0
Ag	0.0	0.0
Co	0.0	0.0
Cr	0.0	0.0

Spectrum 3

	Wt%	σ
C	79.6	0.6
N	11.1	0.7
O	6.1	0.2
F	3.0	0.1
P	0.1	0.0
Ni	0.1	0.0
Co	0.0	0.0
Ag	0.0	0.0
Cr	0.0	0.0
Fe	0.0	0.0

Figure S21. SEM-EDS analysis of a representative working electrode surface after a 30-minute CO_2RR electrolysis using bare glassy carbon electrode with 11.00 M H_2O and 0.1 M *n*Bu_4PF_6 in acetonitrile at -1.95 V vs. Fc/Fc^+.

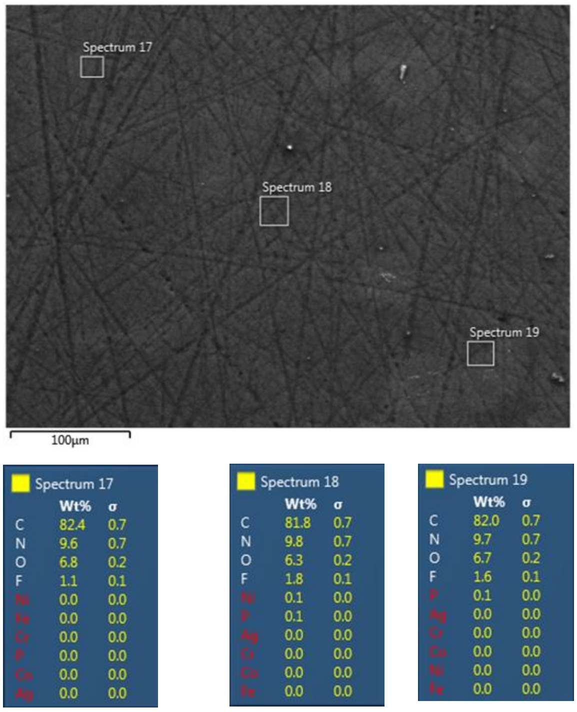

Spectrum 17

	Wt%	σ
C	82.4	0.7
N	9.6	0.7
O	6.8	0.2
F	1.1	0.1
Ni	0.0	0.0
Fe	0.0	0.0
Cr	0.0	0.0
P	0.0	0.0
Co	0.0	0.0
Ag	0.0	0.0

Spectrum 18

	Wt%	σ
C	81.8	0.7
N	9.8	0.7
O	6.3	0.2
F	1.8	0.1
Ni	0.1	0.0
P	0.1	0.0
Ag	0.0	0.0
Cr	0.0	0.0
Co	0.0	0.0
Fe	0.0	0.0

Spectrum 19

	Wt%	σ
C	82.0	0.7
N	9.7	0.7
O	6.7	0.2
F	1.6	0.1
P	0.1	0.0
Ag	0.0	0.0
Cr	0.0	0.0
Co	0.0	0.0
Ni	0.0	0.0
Fe	0.0	0.0

Figure S22. SEM-EDS analysis of a representative working electrode surface after a 30-minute CO_2RR electrolysis using bare glassy carbon electrode with 5.50 M TFE and 0.1 M *n*Bu_4PF_6 in acetonitrile at -1.85 V vs. Fc/Fc^+

Turnover Frequency (TOF) calculations

Method 1:

*TOF*s for CO are calculated based on the total amount of CO generated divided by the total amount of the catalyst in the electrolysis solution and the time of the electrolysis.

$$TOF = \frac{\frac{n(CO)}{n(Cat)}}{t}$$

$n(CO)$ is the total number of moles of CO produced, $n(Cat)$ is the number of moles of the catalyst in the solution, and t is the electrolysis time in seconds.

$n(CO)$ is calculated based on the amount of electrons used specifically for CO generation divided by a factor $2F$ (it is a two-electron reduction reaction from CO_2 to CO):

$$n(CO) = \frac{Q \times FE(CO)}{2F}$$

Q is the charge passed in Coulombs (C); $FE(CO)$ is the Faradaic Efficiency of CO in percentage (%); F is Faraday constant (C/mol)

$n(Cat)$ is calculated based on the following equation:

$$n(Cat) = [Cat] \times V_{sol}$$

$[Cat]$ is the concentration of the catalyst (mol/L); $V_{sol}$is the volume of the solution (L)

Method 2:

TOF values for CO are calculated from CPE data with the equations described by Savéant et al. [S4],[S5]

A) Calculation of diffusion constants D from cyclic voltammograms

For the homogenous system, the relation between the peak current and scan rate in CV is given by the Randles-Sevcik equation:

$$i_p = 0.4463 \left(\frac{F}{RT}\right)^{\frac{1}{2}} n_p^{\frac{3}{2}} FAD^{\frac{1}{2}} [Cat] v^{\frac{1}{2}}$$

i_p is peak current (A), F is Faraday constant (96500 C/mol), R is the universal gas constant (8.31 $J \cdot K^{-1} \cdot mol^{-1}$), T is temperature (298 K), n_p is the number of electrons transferred (1 for each Co-complex redox process), A is the active surface area of the electrode (A = 0.071 cm^2), D is the diffusion coefficient for the complex (cm^2/s), $[Cat]$ is the concentration of the catalyst (mol/cm^3), and v is the scan rate (V/s).

The diffusion coefficients (D) were calculated from the slopes of $i_p - v^{\frac{1}{2}}$ plots

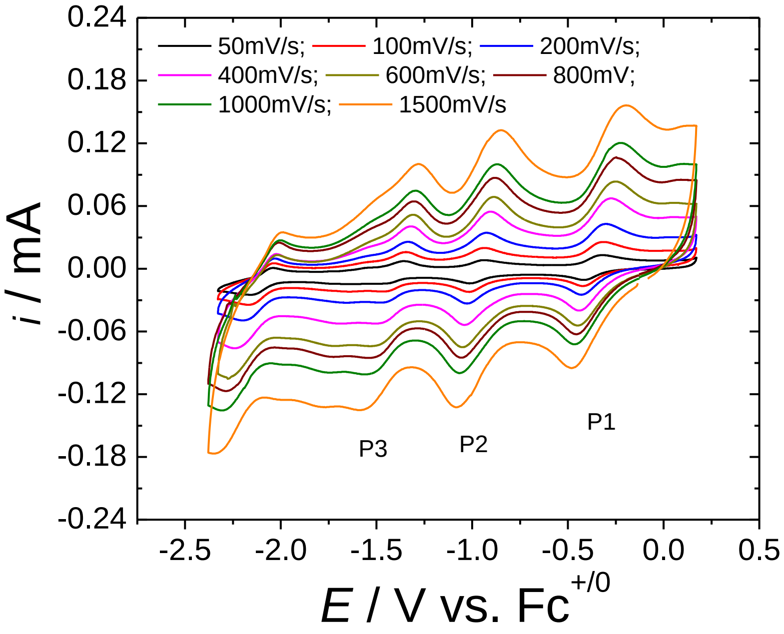

Figure S23. Cyclic voltammograms of the 1.2 mM Cat in MeCN (with 0.1 M *n*Bu_4NPF_6) recorded at different scan rates. The couples of redox peaks P1, P2 and P3 are corresponded to $Co^{3+/2+}$, $Co^{2+/1+}$ and L-L/L-L$^-$ process.

The diffusion coefficient D of the catalyst [Co(L-L)Br_2] could be calculated based on the slopes of the fitted linear curves in Figure S18 and S19, concentration of [Co(L-L)Br_2] and the working electrode surface, using the Randles-Sevcik equation mentioned above. The result is shown in Table S6.

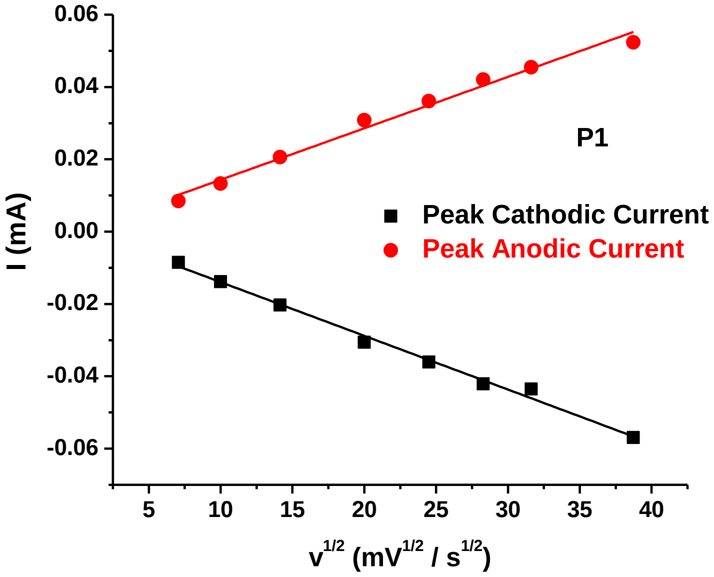

Figure S24. i_p–$v^{1/2}$ plots of P1 ($Co^{3+/2+}$ redox process)

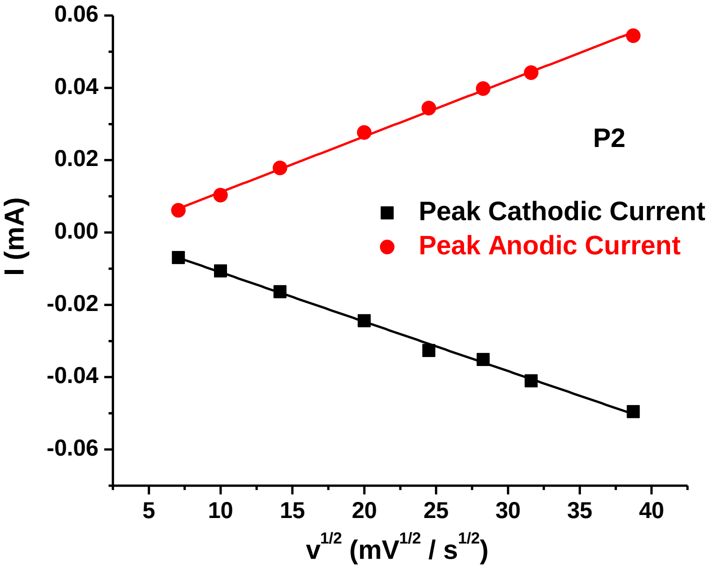

Figure S25. i_p–$v^{1/2}$ plots of P2 ($Co^{2+/1+}$ redox process)

Table S9. The calculation of the diffusion coefficient D for the catalyst

Peak	slope / $(mV/s)^{1/2}$	[Cat] / mM	A /cm^2	D /cm^2/s	D(average)/ cm^2/s
P1cathodic	0.00149	1.2	0.071	4.24×10^{-6}	4.05×10^{-6}
P1anodic	0.00142	1.2	0.071	3.85×10^{-6}	
P2cathodic	0.00137	1.2	0.071	3.58×10^{-6}	
P2anodic	0.00154	1.2	0.071	4.53×10^{-6}	

B) Calculation of TOF for CO generation derived from CPE data using the equations described by Savéant et al. [3],[4]

$$TOF = \frac{\frac{n(CO)}{n(Cat)}}{t}$$

TOF values for CO generation were calculated from the CPE data as reported by Saveant and co-workers.[3],[4],[15] In the homogeneous case, $n(Cat)$ is obtained by space integration of catalyst amount in the reaction-diffusion layer near the surface of the working electrode. $n(CO)$ is calculated based on the charge specially used for CO generation.

$$n(Cat) = A\sqrt{\frac{D}{k_{cat}}}[Cat] = A\sqrt{\frac{D}{TOF_{max}}}[Cat]$$

$$n(CO) = \frac{Q_{el} \times FE}{F}$$

A is the active surface area of the working electrode (2.56 cm^2), D is the diffusion coefficient for the complex (4.05×10^{-6} cm^2/s), k_{Cat} is the reaction rate of catalysis process, TOF_{mas} is the maximum turnover frequency obtained from CVs. It is used to replace k_{Cat} in the calculation, $[Cat]$ is the concentration of the catalyst (0.3×10^{-6} mol/cm^3), F is Faraday constant (96500 C/mol).

So the expression of TOF is:

$$TOF = \frac{\frac{n(CO)}{n(Cat)}}{t} = \frac{\frac{\frac{Q_{el} \times FE}{F}}{A\sqrt{\frac{D}{TOF_{max}}}[Cat]}}{t}$$

$$i_{el} = \frac{Q_{el} \times FE}{t}$$

$$TOF = \frac{i_{el}}{FA}\frac{\sqrt{TOF_{max}}}{\sqrt{D}[Cat]}$$

i_{el} is average current of CPE for CO generation (A), Q_{el} is the charge passed in 30-min CPE (C), FE is the faradaic efficiency of CO (%), t is the time of CPE (s).

The equations below were used for the calculation under the assumption that the electron transfer process to the catalyst is fast and the Nernst equation is obeyed.

$$TOF = \frac{TOF_{max}}{1 + exp\left[\frac{F}{RT}\left(E_{app} - E_{1/2}\right)\right]}$$

R is the universal gas constant (8.31 $J \cdot K^{-1} \cdot mol^{-1}$), T is temperature (298 K), E_{app} is the applied potential during electrolysis (V), $E_{1/2}$ is the redox potential of the ligand (1.65V).

Combination of the equations above gives:

$$TOF = \frac{i_{el}^2\left(1 + exp\left[\frac{F}{RT}\left(E_{app} - E_{1/2}\right)\right]\right)}{F^2A^2D[Cat]^2}$$

Long-time CPE experiments

Table S10. Conditions and Product Analysis of the long-time CPE control groups for CO_2 reduction of 0.3 mM Co(L-L)Br_2

T/min	**E /V vs. FeCp2**	**[Proton source]**	**Charge /C**	**TOF^a/s^{-1}**	**TOF^b/s^{-1}**	**Faradaic Efficiency /%**		**Co / wt%^{c}**
						CO	**H_2**	
60	-1.95	[H_2O] 11.00 M	14.4	3.0×10^{-3}	560	88.2	1.6	0.83 %
90	-1.95	[H_2O] 11.00 M	21.6	2.7×10^{-3}	448	78.9	3.5	1.53 %
120	-1.95	[H_2O] 11.00 M	28.5	1.0×10^{-3}	61.3	29.5	18.7	7.20 %
120	-1.85	[TFE] 5.5 M	31.4	0.8×10^{-3}	34.9	20.2	7.9	4.43 %

[a]TOF is the turnover frequency for CO calculated based on total concentration of catalyst in solution, and therefore is a significant underestimate of catalytic activity. [b]TOF is the turnover frequency for CO generation, derived from CPE data using the equations described by Savéant et al. [c]Weight percent of Co deposited onto the electrode post-electrolysis as measured by SEM-EDS

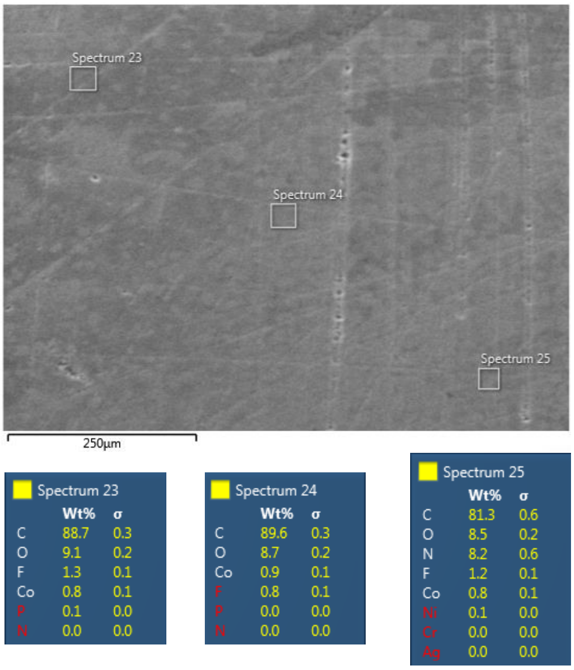

Spectrum 23

	Wt%	σ
C	88.7	0.3
O	9.1	0.2
F	1.3	0.1
Co	0.8	0.1
P	0.1	0.0
N	0.0	0.0

Spectrum 24

	Wt%	σ
C	89.6	0.3
O	8.7	0.2
Co	0.9	0.1
F	0.8	0.1
P	0.0	0.0
N	0.0	0.0

Spectrum 25

	Wt%	σ
C	81.3	0.6
O	8.5	0.2
N	8.2	0.6
F	1.2	0.1
Co	0.8	0.1
Ni	0.1	0.0
Cr	0.0	0.0
Ag	0.0	0.0

Figure S26. SEM-EDS analysis of the working electrode surface after a 60-minute CO_2RR electrolysis using 0.3 mM [Co(L-L)Br_2] with 11.00 M H_2O in acetonitrile at -1.95 V vs. Fc/Fc^+

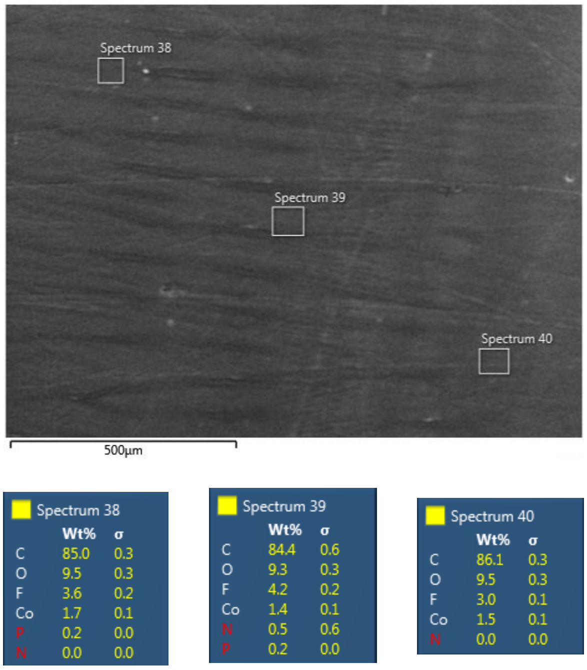

Spectrum 38	Wt%	σ
C	85.0	0.3
O	9.5	0.3
F	3.6	0.2
Co	1.7	0.1
P	0.2	0.0
N	0.0	0.0

Spectrum 39	Wt%	σ
C	84.4	0.6
O	9.3	0.3
F	4.2	0.2
Co	1.4	0.1
N	0.5	0.6
P	0.2	0.0

Spectrum 40	Wt%	σ
C	86.1	0.3
O	9.5	0.3
F	3.0	0.1
Co	1.5	0.1
N	0.0	0.0

Figure S27. SEM-EDS analysis of the working electrode surface after a 90-minute CO_2RR electrolysis using 0.3 mM $[Co(L\text{-}L)Br_2]$ with 11.00 M H_2O in acetonitrile at -1.95 V vs. Fc/Fc^+

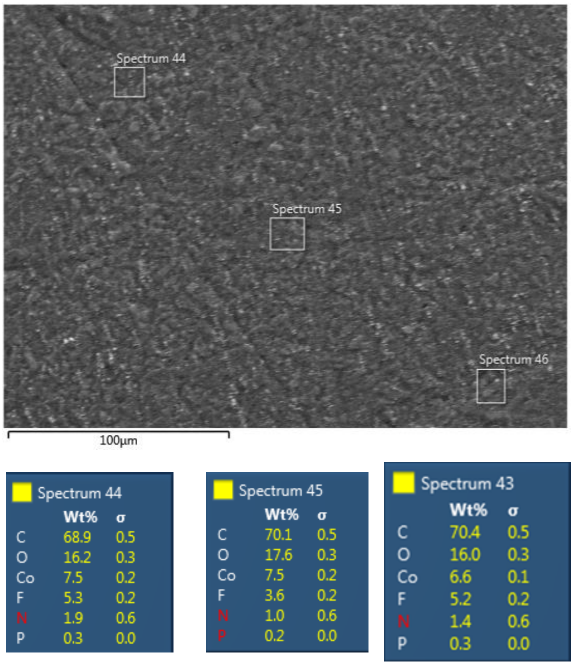

Spectrum 44	Wt%	σ
C	68.9	0.5
O	16.2	0.3
Co	7.5	0.2
F	5.3	0.2
N	1.9	0.6
P	0.3	0.0

Spectrum 45	Wt%	σ
C	70.1	0.5
O	17.6	0.3
Co	7.5	0.2
F	3.6	0.2
N	1.0	0.6
P	0.2	0.0

Spectrum 43	Wt%	σ
C	70.4	0.5
O	16.0	0.3
Co	6.6	0.1
F	5.2	0.2
N	1.4	0.6
P	0.3	0.0

Figure S28. SEM-EDS analysis of the working electrode surface after a 120-minute CO_2RR electrolysis using 0.3 mM $[Co(L\text{-}L)Br_2]$ with 11.00 M H_2O in acetonitrile at -1.95 V vs. Fc/Fc^+

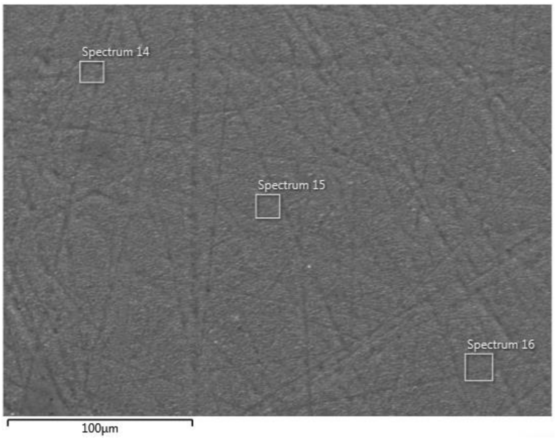

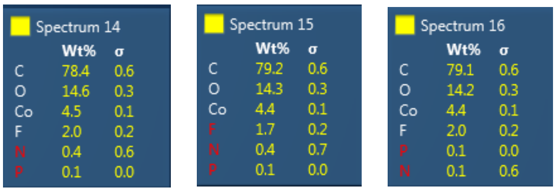

Spectrum 14

	Wt%	σ
C	78.4	0.6
O	14.6	0.3
Co	4.5	0.1
F	2.0	0.2
N	0.4	0.6
P	0.1	0.0

Spectrum 15

	Wt%	σ
C	79.2	0.6
O	14.3	0.3
Co	4.4	0.1
F	1.7	0.2
N	0.4	0.7
P	0.1	0.0

Spectrum 16

	Wt%	σ
C	79.1	0.6
O	14.2	0.3
Co	4.4	0.1
F	2.0	0.2
P	0.1	0.0
N	0.1	0.6

Figure S29. SEM-EDS analysis of the working electrode surface after a 120-minute CO_2RR electrolysis using 0.3 mM [Co(L-L)Br_2] with 5.50 M TFE in acetonitrile at -1.85 V vs. Fc/Fc^+

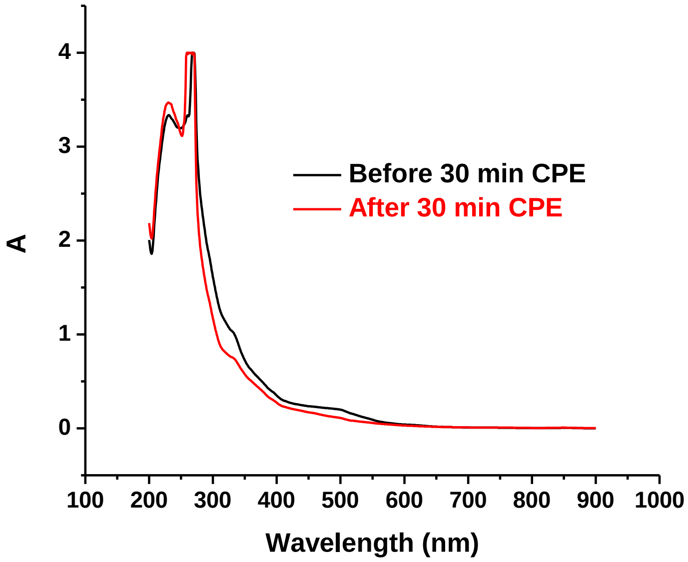

Figure S30. The UV-vis spectra of the acetonitrile solution of 0.3 mM [Co(L-L)Br_2] with 11.00 M H_2O at -1.95 V vs. Fc/Fc^+ before and after 30-minute CPE for CO_2RR

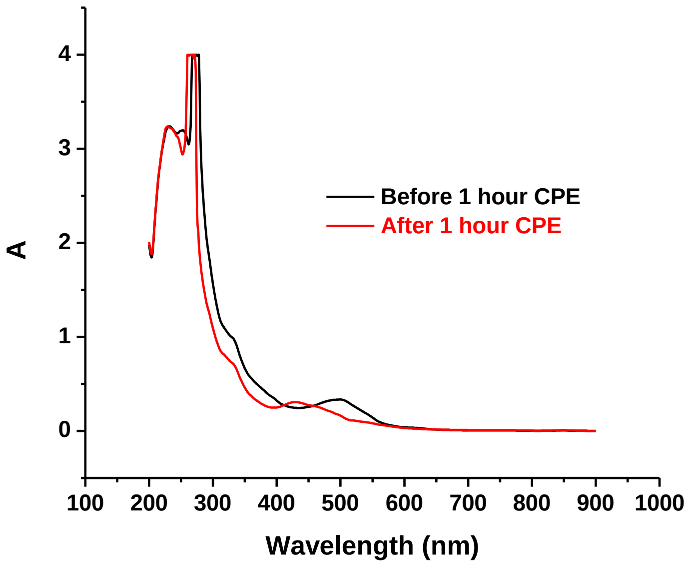

Figure S31. The UV-vis spectra of the acetonitrile solution of 0.3 mM [Co(L-L)Br_2] with 11.00 M H_2O at -1.95 V vs. Fc/Fc^+ before and after 1 hour CPE for CO_2RR

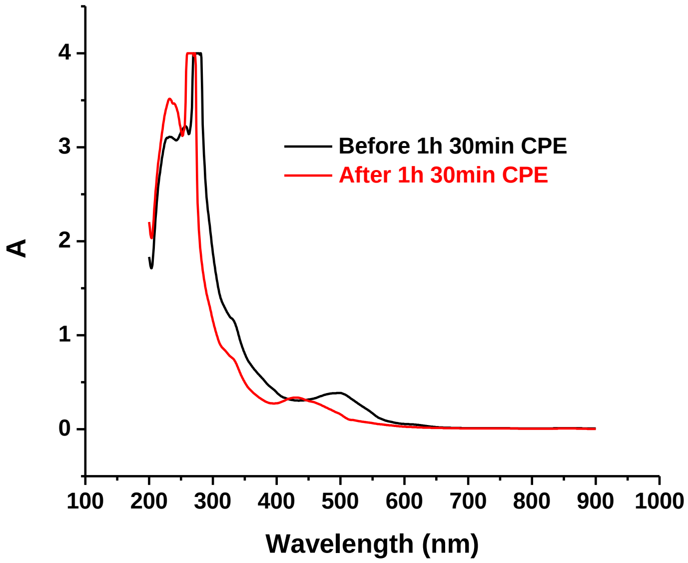

Figure S32. The UV-vis spectra of the acetonitrile solution of 0.3 mM [Co(L-L)Br_2] with 11.00 M H_2O at -1.95 V vs. Fc/Fc^+ before and after 1.5 hour CPE for CO_2RR

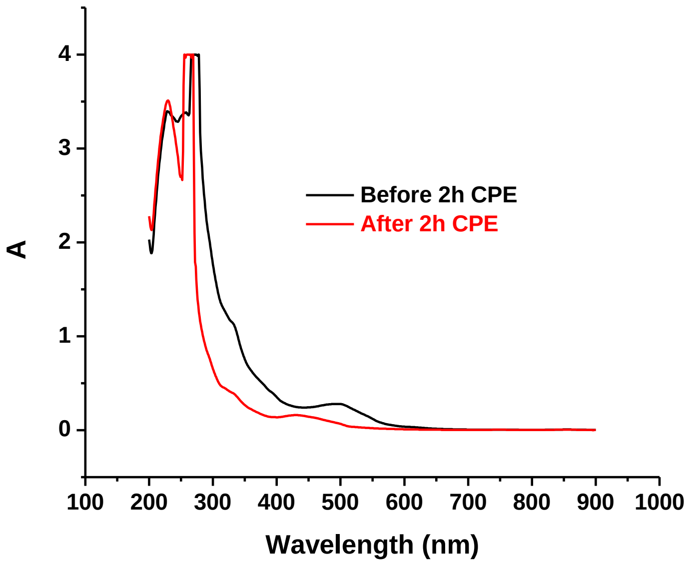

Figure S33. The UV-vis spectra of the acetonitrile solution of 0.3 mM [Co(L-L)Br_2] with 11.00 M H_2O at -1.95 V vs. Fc/Fc^+ before and after 2 hour CPE for CO_2RR

Table S11. Summary of Co-complex catalysts for electrochemical CO_2RR

Catalyst	**CO_2RR E_{onset} /V vs. Fc^+/Fc**	**CPE condition**	**CO_2RR $E_{applied}$ /V vs. Fc^+/Fc**	**TOF /s^{-1} [a]**	**TOF /s^{-1} [b]**	**TOF /s^{-1} [c]**	**Product selectivity**	**Ref.**
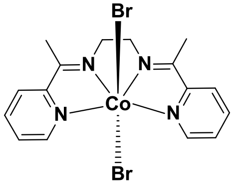	-1.65	0.3 mM Cat in MeCN(0.1 M *n*Bu_4NPF_6) CO_2 with 11M H_2O	-1.95	(3.2 ± 0.4) × 10^{-3}	620	-[d]	CO (80.5%) : H_2 (1.1%) : HCOOH (0.7%)	This work
			-2.15	(8.1 ± 1.3) × 10^{-3}	3961	-	CO (104.3%) : H_2 (0.6%)	
		0.3 mM Cat in MeCN(0.1 M *n*Bu_4NPF_6) CO_2 with 5.5M TFE	-1.85	(4.2 ± 0.5) × 10^{-3}	1089	-	CO (87.7%) : H_2 (1.7%)	
			-2.05	(8.2 ± 0.9) × 10^{-3}	4131	-	CO (102.7%) : H_2(1.0%)	
Other Cobalt Complexes								
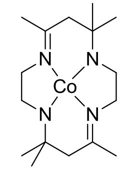	-	1.2 mM Cat 0.1 M KNO, in H_2O/CH,CN 2: 1 (v/v) or H_2O only	-2.00	2.2 × 10^{-3}	-	-	CO (46.5%) : H_2(46.5%)	[S6]
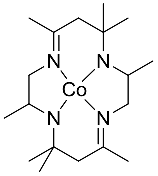	-		-1.90	2.5 × 10^{-3}	-	-	CO (45.0%) : H_2(45.0%)	
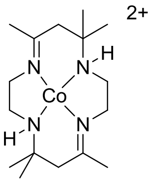	~-1.8	0.18-0.21 mM Cat mercury electrode DMF/H_2O (95/5 v/v) 0.1 M Et_4NCl. H_2O	-1.70	-	-	-	CO (7.9%) : H_2(13.1%)	[S7]
			-2.0		-	-	CO (56.2%) : H_2(25.0%)	

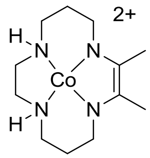	~-1.8	0.18-0.21 mM Cat mercury electrode DMF/H_2O (95/5 v/v) 0.1 M Et_4NCl. H_2O	-2.0	-	-	-	CO (13.3%) : H_2(58.8%)	[S7]
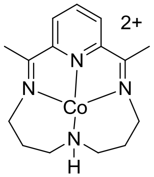	~-1.8		-1.7	-	-	-	CO (66.4%) : H_2(5.3%)	
			-2.0	-	-	-	CO (41.5%) : H_2(10.9%)	
$[Co(tpy)_2]^{2+}$ tpy: 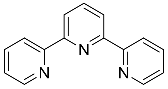	~-2.03	2 mM Cat CO2-saturated DMF/ H2O (95 : 5, v : v) with 0.1 M TBAP	-1.93	-	-	-	CO (20.0%) : H_2(1.0%)	[S8]
			-2.03	-	-	-	CO (12.0%) : H_2(5.0%)	
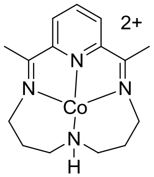	~-1.55	0.3 mM Cat MeCN(0.1 M $n$$Bu_4NPF_6$) CO_2 with 10M H_2O	-2.13	1.7×10^{-3}	-	-	CO (45.0%) : H_2(30.0%)	[S9]
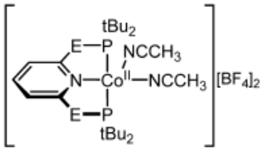 E = CH_2	~-2.1	1.0 mM Cat in CH_3CN with 0.20 M Bu_4NBF_4	-	-	-	-	-	[S10]
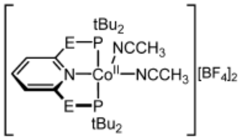 E = NH	~-2.5		-	-	-	-	-	

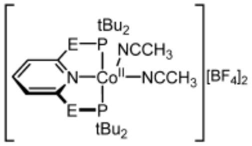 E = O	~-2.2	1.0 mM Cat in CH_3CN with 0.20 M Bu_4NBF_4	-	-	-	-	-	-	[S10]
[Co^{II}(TPA)Cl][Cl] TPA: 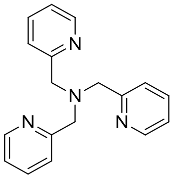	~-1.94	MeCN(0.1 M $n$$Bu_4NPF_6$)	-	-	-	-	-	-	[S11]
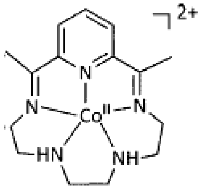	~-1.7	1.0 mM Cat in DMF, 0.1M $n$$Bu_4NPF_6$	-1.9	-	-	-	-	CO (82.0%)	[S12]
[Co^{II}(L-R)(solv1)(solv2)] 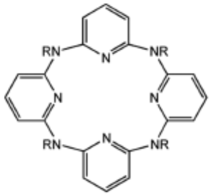 L-R: R = H; solv1 = solv 2 = acetone	-2.36	0.5 mM Cat in DMF, 0.1M $n$$Bu_4NPF_6$ CO_2 with 1.2M TFE	-2.8	0.86×10^{-3}	170	360		CO (98.0%)	[S13]
[Co^{II}(L-R)(solv1)(solv2)] R = Me; solv1 = MeCN solv 2 = none	-2.58	0.5 mM Cat in DMF, 0.1M $n$$Bu_4NPF_6$ CO_2 with 1.2M TFE	-2.8	0.04×10^{-3}	0.5	78		CO (23.0%)	

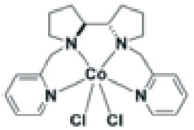 *cis*-[Co^{II}(PDP)Cl$_2$]	-1.95	1 mM Cat in MeCN, 0.1M *n*Bu$_4$NPF$_6$ CO$_2$	-2.1	-	-	-	30min: CO (96.0%) 4 hours: CO (85.0%)	[S14]
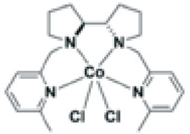 *cis*-[Co^{II}(DMPDP)Cl$_2$]	-1.93	1 mM Cat in MeCN, 0.1M *n*Bu$_4$NPF$_6$ CO$_2$	-2.1	low	low	-	-	
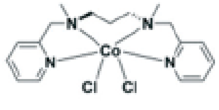 *cis*-[Co^{II}(PDMBP)Cl$_2$]	-1.97	1 mM Cat in MeCN, 0.1M *n*Bu$_4$NPF$_6$ CO$_2$	-2.1	low	low	-	-	
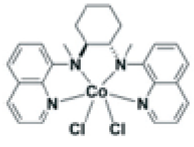 *cis*-[Co^{II}(BQCN)Cl$_2$]	-1.87	1 mM Cat in MeCN, 0.1M *n*Bu$_4$NPF$_6$ CO$_2$	-2.1	low	low	-	-	
[Co(TPA)X]$^+$ TPA: 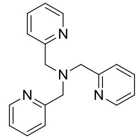 X = Cl	-1.96	in MeCN, 0.1M *n*Bu$_4$NPF$_6$ CO$_2$	-	-	-	-	-	[S15]
[Co(TPA)X]$^+$ X = Br	-1.83		-	-	-	-	-	
[Co(TPA)X]$^+$ X = I	-1.72	in MeCN, 0.1M *n*Bu$_4$NPF$_6$ CO$_2$	-	-	-	-	-	

$[Co(TPA)X]^+$ X = NCS	-1.76		-	-	-	-	-	
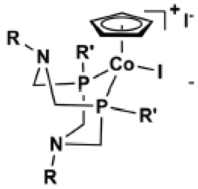 1(R’= Cy; R=Bn)	-2.08	0.5 mM Cat in DMF, 0.1M $n$$Bu_4NPF_6$ CO_2 with 1.1M H_2O	-2.10	2.2×10^{-3}	70	-	HCOOH(92%): CO (<1%) : H_2(5%)	[S16]
			-2.25	7.2×10^{-3}	650	-	HCOOH(98%): CO (<1%) : H_2(5%)	
2(R’= Cy; R=Ph)	-2.0	0.5 mM Cat in DMF, 0.1M $n$$Bu_4NPF_6$ CO_2 with 1.1M H_2O	-2.05	1.4×10^{-3}	60	-	HCOOH(94%): CO (1%) : H_2(3%)	
			-2.20	2.5×10^{-3}	180	-	HCOOH(98%): CO (<1%) : H_2(4%)	
3(R’= Ph; R=Bn)	-1.93	0.5 mM Cat in DMF, 0.1M $n$$Bu_4NPF_6$ CO_2 with 1.1M H_2O	-2.00	0.5×10^{-3}	20	-	HCOOH(88%): CO (<1%) : H_2(8%)	
			-2.05	1.0×10^{-3}	40	-	HCOOH(86%): CO (<1%) : H_2(6%)	
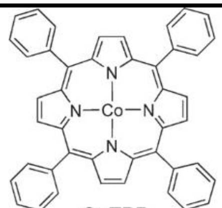 CoTPP	-2.20	1 mm CoTPP in DMF, 0.1M $n$$Bu_4NPF_6$ CO_2 with	-2.35	2.6×10^{-4}	-	-	CO (50.0%) : H_2(2.0%): HCOOH(4%): Acetate(2%): Oxlate(0.2%)	[S17]

[a]TOF is the turnover frequency for CO calculated based on total concentration of catalyst in solution, and therefore is a significant underestimate of catalytic activity (See TOF method 1 in page 18). Included for comparison purposes only. [b]TOF is the turnover frequency for CO generation, derived from CPE data using the equations described by Savéant et al. (See TOF method 2 in page 18).[S4],[S5] [c]TOF is the turnover frequency derived from CV experiments. [d]Not measured

Reference

[S1] C. C. L. McCrory, N. K. Szymczak, and J. C. Peters, *Electrocatalysis*, 2016, **7**, 87-96.

[S2] *SHELXTL (version 5.0), Reference Manual*, Siemens Industrial Automation, Analytical Instruments, Madison, WI, 1995.

[S3] S. Gourbatsis, S. P. Perlepes, N. Hadjiliadis, *Transition Met. Chem.*, 1990, **15**, 300.

[S4] C. Costentin, M. Robert, J.-M. Saveant, *Chem. Soc. Rev.*,2013, **42**, 2423.

[S5] C. Costentin, S. Drouet, M. Robert, J.-M. Savéant, *Science*, 2012, **338**, 90

[S6] B. J. Fisher, R. Eisenberg, *J. Am. Chem. Soc.*, 1980, **102**, 7361

[S7] A. H. A. Tinnemans, T. P. M. Koster, D. H. M. W. Thewissen, A. Mackor, *Rec. Trav. Chim. Pays Bas*, 1984, **103**, 288.

[S8] N. Elgrishi, M. B. Chambers, V. Artero, M. Fontecave, *Phys. Chem. Chem. Phys.* 2014, **16**, 13635

[S9] D. C. Lacy, C. C. L. McCrory, J. C. Peters, *Inorg. Chem* 2014, **53**, 4980

[S10] D. W. Shaffer, S. I. Johnson, A. L. Rheingold, J. W. Ziller, W. A. Goddard, R. J. Nielsen, J. Y. Yang, , *Inorg. Chem* 2014, **53**, 13031.

[S11] S. L.-F. Chan, T. L. Lam, C. Yang, S.-C. Yan, N. M. Cheng, *Chem. Commun.* 2015, **51**, 7799

[S12] L. Chen, Z. Guo, X.-G. Wei, C. Gallenkamp, J. Bonin, E. Anxolabéhère-Mallart, K.-C. Lau, T.-C. Lau, M. Robert, *J. Am. Chem. Soc.*, 2015, **137**, 10918.

[S13] A. Chapovetsky, T. H. Do, R. Haiges, M. K. Takase, S. C. Marinescu, *J. Am. Chem. Soc.*, 2016, **138**, 5765.

[S14] F. Wang, B. Cao, W.-P. To, C.-W. Tse, K. Li, X.-Y. Chang, C. Zang, S. L.-F. Chan, C.-M. Che, *Catal. Sci. Technol.*, 2016, **6**, 7408

[S15] S. L.-F. Chan, T. L. Lam, C. Yang, J. Lai, B. Cao, Z. Zhou, Q. Zhu, *Polyhedron* 2017, **125,** 156.

[S16] S. Roy, B. Sharma, J. Pécaut, P. Simon, M. Fontecave, P. D. Tran, E. Derat, V. Artero, *J. Am. Chem. Soc.*, 2017, **139**, 3685.

[S17] X-M. Hu, M. H. Rønne, S. U. Pedersen, T. Skrydstrup, K. Daasbjerg. *Angew. Chem. Int. Ed.* 2017, ***56***, 6468.

[S18] M. Popescu, P. Rotaru, M-V. Bubulica, A. Kriza, *J. Therm. Anal. Calorim.*, 2015, ***120***, 641.

[S19] B. D. Stubbert, J. C. Peters, H. B. Gray, *J. Am. Chem. Soc.* 2011, ***133***, 18070.

[S20] D.F. Evans, *J. Chem. Soc.*, 1959, **0**, 2003.